Journal of Medicinal Chemistry

pubs.acs.org/jmc

Drug Annotation

Discovery of TAK-981, a First-in-Class Inhibitor of SUMO-Activating Enzyme for the Treatment of Cancer

Steven P. Langston,* Stephen Grossman,* Dylan England, Roushan Afroze, Neil Bence, Douglas Bowman, Nancy Bump, Ryan Chau, Bei-Ching Chuang, Christopher Claiborne, Larry Cohen, Kelly Connolly, Matthew Duffey, Nitya Durvasula, Scott Freeze, Melissa Gallery, Katherine Galvin, Jeffrey Gaulin, Rachel Gershman, Paul Greenspan, Jessica Grieves, Jianping Guo, Nanda Gulavita, Shumet Hailu, Xingyue He, Kara Hoar, Yongbo Hu, Zhigen Hu, Mitsuhiro Ito, Mi-Sook Kim, Scott Weston Lane, David Lok, Anya Lublinsky, William Mallender, Charles McIntyre, James Minissale, Hirotake Mizutani, Miho Mizutani, Nina Molchinova, Koji Ono, Ashok Patil, Mark Qian, Jessica Riceberg, Vaishali Shindi, Michael D. Sintchak, Keli Song, Teresa Soucy, Yana Wang, He Xu, Xiaofeng Yang, Agatha Zawadzka, Ji Zhang, and Sai M. Pulukuri

Cite This: *J. Med. Chem.* 2021, 64, 2501−2520

Read Online

ACCESS | Metrics & More | Article Recommendations | Supporting Information

ABSTRACT: SUMOylation is a reversible post-translational modification that regulates protein function through covalent attachment of small ubiquitin-like modifier (SUMO) proteins. The process of SUMOylating proteins involves an enzymatic cascade, the first step of which entails the activation of a SUMO protein through an ATP-dependent process catalyzed by SUMO-activating enzyme (SAE). Here, we describe the identification of TAK-981, a mechanism-based inhibitor of SAE which forms a SUMO−TAK-981 adduct as the inhibitory species within the enzyme catalytic site. Optimization of selectivity against related enzymes as well as enhancement of mean residence time of the adduct were critical to the identification of compounds with potent cellular pathway inhibition and ultimately a prolonged pharmacodynamic effect and efficacy in preclinical tumor models, culminating in the identification of the clinical molecule TAK-981.

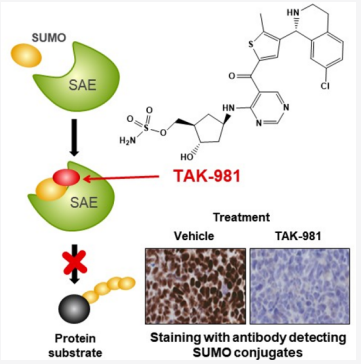

INTRODUCTION

Small ubiquitin-like modifier (SUMO) proteins are reversible post-translational modifiers of intracellular proteins. The SUMOylation of proteins occurs through a three-step enzymatic cascade involving activation, transfer, and ligation of SUMO protein to lysine residues of target proteins. The first step of the cascade is catalyzed by SUMO activating enzyme (SAE), which belongs to a small family of activating enzymes collectively known as E1s.[1,2] SAE is a heterodimeric protein (SAE1, SAE2, or UBA2) and activates SUMO proteins through the carboxy terminus by reaction with ATP to form an acyl adenylate intermediate that is primed for acylation of a cysteine residue on the enzyme to form a thioester. The SUMO protein is subsequently transferred, through thioester exchange, to the SUMO specific conjugating enzyme E2, UBC9.[3,4] Aided by SUMO specific E3 protein ligases, the SUMO proteins are transferred to lysine residues of target proteins to form oligomers through formation of an isopeptide bond.[5] The enzymatic cascade is shown in Scheme 1, steps A−C. This three-step sequence is analogous to the process of ubiquitination and neddylation of cellular proteins, the first step of which is catalyzed by the homologue E1 ubiquitin activating enzyme (UAE) or Nedd8 activating enzyme (NAE), respectively.[6,7]

There are three SUMO family members: SUMO1, which conjugates to target proteins as a monomer, and SUMO2 and SUMO3, which modify proteins through formation of oligomeric chains.[5] The modification of proteins by SUMO alters their molecular surface and can have effects on the protein's catalytic activity, cellular localization, and interaction with other proteins. In recent years, protein targets of SUMOylation have been identified that play key roles in multiple cellular pathways, including cell division and DNA repair, nuclear transport, gene transcription, chromosome structure and segregation, and immune response modulation.[1,8]

Received: October 27, 2020
Published: February 25, 2021

https://dx.doi.org/10.1021/acs.jmedchem.0c01491
J. Med. Chem. 2021, 64, 2501−2520

Scheme 1. Enzymatic Cascade for the SUMOylation of Target Proteins and Mechanism of Inhibition of Adenosine Sulfamate Analogues

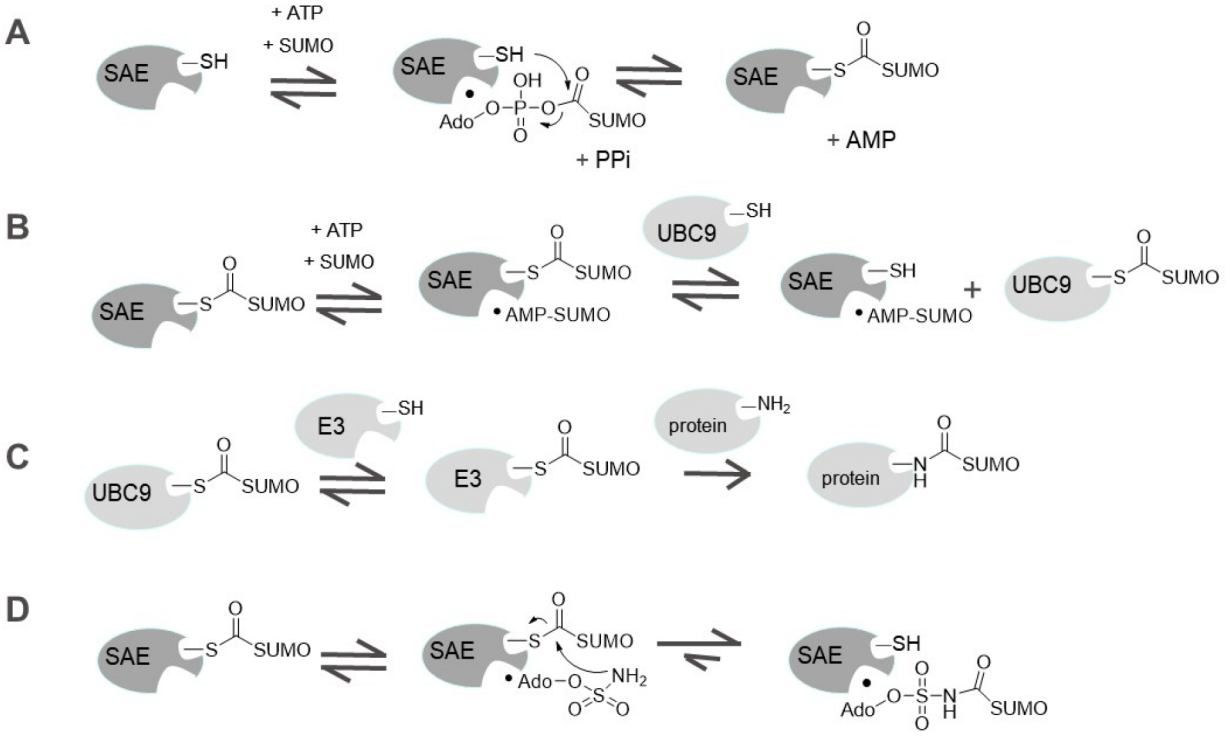

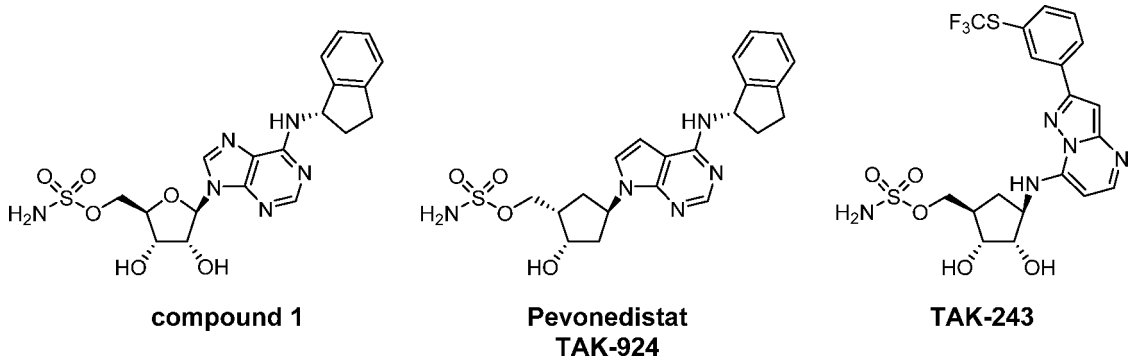

Figure 1. An early adenosine sulfamate and clinical compounds for NAE and UAE.

Elevated levels of the components of the SUMO pathway, e.g. UBC9, are associated with poor patient outcome in certain malignancies.[9,10] Knockdown of SAE has been reported to confer synthetic lethality in cell lines and tumor models with high myc expression, and shRNAs targeting components of the SUMO pathway have demonstrated tumor growth inhibition in xenograft models.[11−14] SUMOylation has also been shown to modulate innate immune responses.[15] A net inhibitory effect of SUMOylation on type 1 interferon (IFN) expression has been demonstrated such that inhibiting SUMOylation by genetic means resulted in enhanced basal expression levels and sensitization of induction of type 1 IFNs by pathogenic stimuli.[16,17]

In addition, SUMOylation has been found to suppress a type1 interferon response to innate immune sensors, and depletion of UBC9 in hematopoietic cells enhanced an inflammatory response and protection to viral infection in mouse models.[16,17] Collectively, these observations warrant the identification of potent and selective small molecule inhibitors of SAE to explore the cellular effects of SUMO pathway inhibition and potential therapeutic opportunity.

RESULTS AND DISCUSSION

Our group has previously identified a class of adenosine sulfamate (AdoS) derived inhibitors of E1 enzymes that act through a unique type of mechanism-based inhibition termed substrate assisted inhibition.[18,19] These inhibitors were shown to act through reaction of the sulfamate moiety with a cysteine thioester of the E1 enzyme and UBL to form a UBL−inhibitor adduct within the enzyme catalytic site, Scheme 1 step D, using SAE as an illustrative example. The conformation of the enzyme that binds the substrates ATP and SUMO is thought to be open, while a more closed structure resembling that captured in the crystal structure of a SUMO-adenosine vinylsulfone covalently trapped intermediate may also contribute to binding the SUMO-AdoS adduct.[20,21]

An early example of the series is the N-6 substituted adenosine sulfamate compound **1**, a nonselective E1 inhibitor, was shown

https://dx.doi.org/10.1021/acs.jmedchem.0c01491
J. Med. Chem. 2021, 64, 2501−2520

Table 1. Enzyme and Cell Activity of Initial Inhibitors of SAE

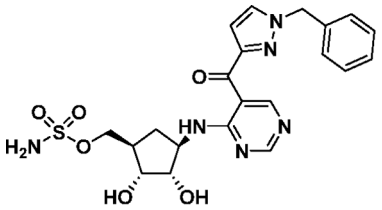

2

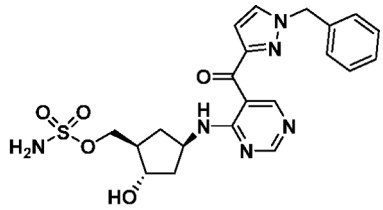

3

	HTRF, IC_{50} nM[a]			ATP-PPi, IC_{50} nM[b]			Western blot, IC_{50} nM[c]		
compound	SAE	UAE	NAE	SAE (SUMO1/2)	UAE	NAE	SUMO-UBC9	Ub-UBC12	Nedd 8-UBC10
2	1	58	29	6/50	1100	300	6	410	1400
3	2	>1000	190	11/69	>1000	2600	13	2600	>5000

[a]Transthiolation assay measuring inhibition of the transfer of SUMO1 to UBC9 (the E2 for SAE) at an [ATP] approximating K_m (20 μM). [b]Pyrophosphate exchange assay measuring inhibition of enzyme activity for either SUMO1 or SUMO2 substrates for SAE, Ub for UAE, and Nedd-8 for NAE; all were conducted at 1 mM [ATP]. [c]Cellular assay conducted in HCT116 cells assessing inhibition of conjugation (transthiolation) of SUMO proteins to UBC9. Similarly, for conjugation of ubiquitin to UBC12 and conjugation of Nedd-8 to UBC-10, the UBL and E2 substrates for UAE and NAE, respectively.

to be capable of forming an inhibitor adduct with E1 UBL substrates, including UAE, NAE, and SAE, Figure 1.[18] Compound **1** was optimized through an iterative medicinal chemistry program to the selective inhibitor of NAE, Pevonedistat (TAK-924, MLN-4924), which is currently in clinical trial for solid and heme malignancies, including a phase III trial in combination with azacytidine for patients with high risk myelodysplastic syndrome (HR MDS), chronic myelomonocytic leukemia (CMML), or low-blast acute myeloid leukemia (AML) (NCT03268954).[22−24] Pevonedistat was shown to selectively inhibit NAE by reacting with the NAE-Nedd-8 thioester to form the Nedd-8-Pevonedistat adduct, a tight binding bisubstrate analogue, within the enzyme active site.[18,25] The chemical class was subsequently diversified, and the UAE inhibitor TAK-243 was identified, which acts via a similar mechanism forming a ubiquitin−TAK-243 adduct that inhibits UAE and also entered clinical evaluation within oncology (NCT03816319), Figure 1.[26−29]

Despite demonstrating that compound **1** was able to form SUMO−compound **1** adduct, it proved challenging to identify a selective compound capable of demonstrating robust inhibition of the SUMO pathway in cells. Compounds reported to be inhibitors of SAE were not useful as tool compounds due to weak activity and unclear selectivity.[30−32] While conducting an extensive scaffold hopping exercise within the adenosine sulfamate series, compound **2** was prepared and demonstrated potent SAE activity in the HTRF or transthiolation assay.[19] Although retaining significant activity for UAE and NAE, it was an example of a distinct chemotype, and removal the 2′-hydroxyl (adenosine numbering) gave a somewhat more selective molecule **3**, Table 1. The homogeneous time resolved fluorescence (HTRF) assay was conducted at K_m for ATP and utilized SUMO1 as the UBL substrate. The compounds were also shown to be active at millimolar ATP concentration for both SUMO1 and SUMO2 as substrates by employing a pyrophosphate exchange assay.[19] Importantly, quantitative Western blot assays demonstrated robust inhibition of the SUMO pathway in cells, giving a selective reduction in the concentration of the E2 intermediate UBC9-SUMO compared to the E2-UBL conjugates for UAE and NAE, Table 1 and Figure 2. We were thus encouraged to utilize this scaffold as the basis of a SAR exploration to identify potent and selective inhibitors of

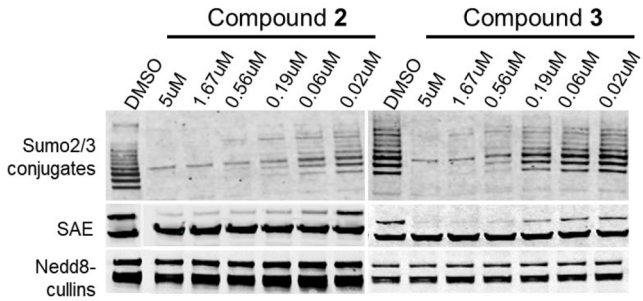

Figure 2. Western blot demonstrating cellular pathway inhibition by compounds **2** and **3**. Inhibition of SAE and NAE in cells was assessed by immunoblot analysis of SUMO2/3-conjugated proteins, SAE enzyme, and neddylated cullin levels in HCT-116 cell lysates. Multiple SUMO2/3 conjugate bands reflect the myriad proteins serving as substrates for SUMOylation.

SAE to explore the biology and potential therapeutic utility of SAE and consequently SUMO pathway inhibition both in cells and *in vivo*.

The Western blot assay served to demonstrate potent, selective pathway inhibition in cells. However, to support a medicinal chemistry program, we required a higher throughput assay that was amenable to automation. In cells, there exists a highly dynamic process of SUMOylation and deSUMOylation.[1] SUMO conjugated proteins, which normally have high molecular weight, are mainly localized within the nucleus. The cellular inhibition of SAE results in an apparent loss of SUMOylated proteins in the nucleus due to rapid deSUMOylation, catalyzed by SUMO specific proteases, coupled with the inability to further SUMOylate existing or newly synthesized proteins. Additionally, free SUMO levels increase and redistribute throughout the cell. An immunofluorescence assay (SUMO IF) was developed to monitor this redistribution of SUMO protein from nucleus to cytosol and quantify SAE inhibition in the HCT116 tumor cell line. Representative images are shown in Figure 3.

Initial SAR investigation focused on two areas of the molecule: exploration of the substitution pattern of the cyclopentane core and N1-substituents of the 3-substituted pyrazole. The 2′-deoxy compound **3** improved selectivity toward NAE and UAE with only a slight decrease in activity,

https://dx.doi.org/10.1021/acs.jmedchem.0c01491
J. Med. Chem. 2021, 64, 2501−2520

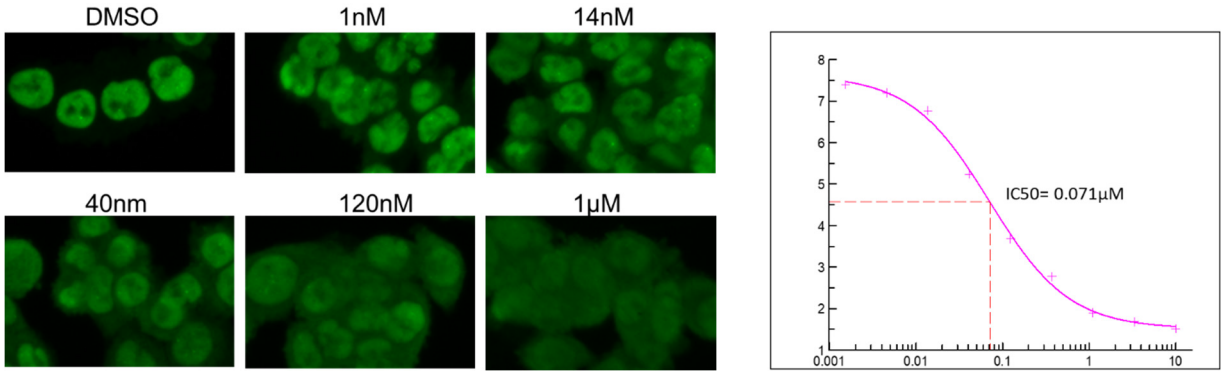

Figure 3. The SUMO2/3 immunofluorescence assay. This assay measures the level of inhibition of the SAE by measuring the ratio of SUMO2/3 in the nuclear versus cytoplasmic cellular compartments. HCT-116 cells were seeded in 96-well plates and treated with compound **3** at the indicated concentrations for 4 h followed by staining with antihuman SUMO2/3 monoclonal antibody (MBL, clone 1E7). Imaging was performed on an IX-Ultra imager and analyzed for SUMO2/3 inner/outer ratio using MetaXpress Translocation-Enhanced module. Dose-dependent reduction of cytoplasmic SUMO2/3 positive staining reflects loss of SUMOylated proteins sequestered in this compartment under physiological conditions (DMSO). Right panel shows the dose response for compound **3** in HCT-116 cells as determined by the SUMO2/3 immunofluorescence assay.

Table 2. SAR Exploration of the Cyclopentyl Ring

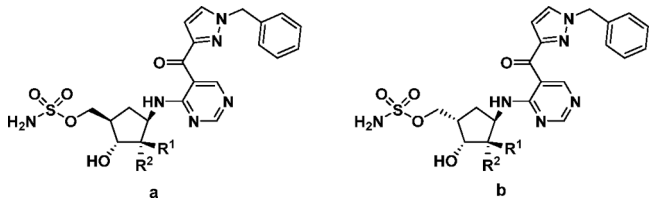

compound	structure	R^1	R^2	IC_{50} (nM) SAE	NAE	UAE	SUMO $IFIC_{50}$ (nM)
2	a	H	OH	1	29	58	26
3	a	H	H	1.8	190	>1000	71
4	a	OH	H	27	748	>1000	1530
5	b	H	H	22	806	>1000	>1000
6	a	H	F	3.8	334	>1000	517
7	a	F	H	2.3	688	492	260
8	a	F	F	3.9	>1000	>1000	249

while epimerization of the alcohol at this position as in **4** reduced activity for all three enzymes, Table 2. Fluorination of the 2′-position was tolerated as either epimer, see **6** and **7**, and as the difluorinated compound **8**, with modest improvements in selectivity, although at the expense of cell potency and added synthetic complexity. Epimerization of the C4′-methylene sulfamate, as in **5**, to give the antirelationship relative to the nucleobase mimetic, reminiscent of the configuration for the NAE inhibitor TAK-924, reduced activity, Table 2.

An array of N1-pyrazole substituents was investigated, see Table 3. The benzyl group was found to be preferred over alkyl groups, including linear and branched alkyl substituents. The benzyl group, as in **3**, was also preferred over phenyl, as in **9**, and the corresponding methylene cyclohexane **10**. Investigating the preferred substitution pattern around the benzyl group showed that the meta-position, as in **12**, for chloro-substitution was preferred over ortho **11** and para **13**, and typically, larger more hydrophobic groups were preferred at this position (ML-792, **15**−**19**). Methylene heterocycles with halo substitution were also found to be potent, for example the 5-chloro-2-furanyl **19**, corresponding thiophene **20**, and the 6-halo-2-pyridines (**21**, **22**), Table 3.

Alternative heterocycles to the 3-pyrazole were also explored. The N-substituted 3-pyrrole was found to be potent although less selective toward NAE; see **23** and **25** compared to **3** and ML-792. The N-benzyl 4-pyrazole regioisomer **24** was less potent than the 3-pyrazole, Table 4. Heterocycles with C-benzylation were also explored, and the 4-benzylated 2-thiophene **26** showed promising potency, especially in the cellular SUMO IF assay, compared to the thiophene and furan isomers **27** and **28**, Table 4.

ML-792 was chosen as a suitable representative compound to investigate the effects of SAE inhibition on cancer cell biology because of its potency and selectivity. The effects of ML-792 on several cancer lines have been previously reported.[33] For the HCT116 cancer cell line, both an apoptotic and senescent phenotype were observed, resulting in a reduced cell proliferation in a 72 h viability assay. The next step was to explore the effects of SAE and SUMO pathway inhibition in in vivo tumor xenograft models. Selective pathway inhibition was first determined by Western blot assays showing loss of SUMO-Ubc9 thioester and SUMO-protein conjugates beyond 8 h following a single subcutaneous dose. The SUMO-ML-792 adduct from xenograft homogenates was quantified initially by mass spectrometry.[18] Subsequently, an antibody to the SUMO-ML-792 adduct was developed to quantify levels of adduct by immunohistochemistry (IHC). Additionally, an IHC assay was developed to assess the levels of SUMO−protein conjugates in

https://dx.doi.org/10.1021/acs.jmedchem.0c01491
J. Med. Chem. 2021, 64, 2501−2520

Table 3. SAR Exploration of Pyrazole Substituents

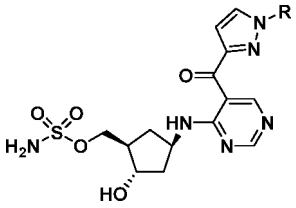

compound	R	IC$_{50}$ (nM) SAE	NAE	UAE	SUMO IF IC$_{50}$ (nM)
9	Ph	67	32	468	>1000
10	cyclohexylmethyl	8.2	276	>1000	1610
11	2-Cl-benzyl	3.2	215	>1000	332
12	3-Cl-benzyl	0.7	242	>1000	20
13	4-Cl-benzyl	5.1	>1000	>1000	1880
14	3-F-benzyl	2.9	357	>1000	515
ML-792	3-Br-benzyl	0.4	228	>1000	10
15	3-Me-benzyl	1.7	308	>1000	29
16	3-ethynylbenzyl	1.1	304	>1000	22
17	3-CF_3-benzyl	1.1	695	>1000	39
18	3-CF_3O-benzyl	2.1	>1000	>1000	78
19	(5-Cl-furan-2-yl) methyl	1.1	435	>1000	33
20	(5-Cl-thiophen-2-yl)methyl	2.0	353	>1000	228
21	(6-Cl-pyridine-2-yl)methyl	1.0	478	>1000	66
22	(6-Br-pyridine-2-yl)methyl	0.7	581	>1000	49

cellular nuclei from xenograft homogenates. This facilitated observation of target engagement (presence of adduct) and SUMO pathway inhibition (loss of SUMO-protein conjugates) in the same tissue. The ratio of nuclei staining positive for SUMO-ML-792 adduct and SUMO−protein conjugates to total nuclei in HCT116 (colorectal carcinoma) xenograft homogenates is plotted in Figure 4. Importantly, an inverse relationship between the persistence of SUMO−inhibitor adduct with the rate of SUMOylated protein recovery was observed. The pathway recovers between 8 and 24 h despite significant adduct remaining. This may be due to partial restoration of enzyme activity through adduct release. The effect on tumor growth was investigated, and we were gratified to observe robust, dose-dependent tumor growth inhibition in the HCT116 model on both continuous and intermittent dosing schedules, Figure 5.

With establishment of PD markers for both target engagement and pathway inhibition as well as robust tumor growth inhibition, we were encouraged to continue to optimize the chemical series. The dose of ML-792 required for a robust PD response and efficacy was high (150 mg/kg s.c.) and involved twice daily administration; thus, we aimed to prolong PD response to dosing frequency. The SAE enzyme is relatively long-lived, and we determined that the resynthesis rate, even in the presence of the SAE inhibitor ML-792, is comparable to cellular doubling time.[33] It was thus anticipated that optimizing the binding affinity of the adduct to the enzyme would increase the residence time of the inhibitory adduct species in the enzyme active site and result in prolonged pathway inhibition.

To support this approach, the SUMO IF assay was adapted to assess duration of pathway inhibition by including a compound washout step. In this format, the cells were incubated with a range of compound concentrations for 2 h. The cells were then washed to remove residual compound, and the nuclear and cytoplasmic SUMO2/3 fluorescence signal was measured immediately or 8 h following washout. As a result of pathway recovery, the SUMO2/3 fluorescence signal was shown to relocalize to the nucleus over time, and an IC$_{50}$ was calculated and reported at 0 and 8 h, Table 5.

Cocrystallization of the enzyme, inhibitor, ATP, and SUMO substrate, using procedures modified from those developed for UAE and NAE, gave high resolution crystal structures of the SUMO−inhibitor adduct for both **2** and **3** within the SAE active site, see Figure 6 for compound **2**.[18] An internal H-bond is apparent between the amino and ketone functionalities, stabilizing the orientation of the pyrimidine and facilitating formation of an H-bond between N1 of the pyrimidine and the backbone NH of Ile96. The pyrazole nitrogen is facing the same direction as the ketone and interacting with Asn118. Replacing the pyrazole with thiophene was anticipated to lead to a similar orientation with the sulfur facing the same direction as the ketone to maximize nonbonding sulfur−oxygen interactions. The 2,4-thiophene substituted system, exemplified in compounds **26** and **29**, was chosen as an alternative starting point for further optimization because, unlike the pyrazole series, it gives the ability to incorporate heteroatoms on the benzylic methylene position which was anticipated to lead to additional H-bond interaction with Ser95, potentially helping to stabilize the adduct within the enzyme and increase residence time, Figure 6.

The 3-chloro benzyl thiophene **29** was 5−10-fold less potent than the pyrazole ML-792 in the cellular SUMO IF assay both at 0 and 8 h following washout, Table 5. Substitution of the benzylic methylene with a hydroxyl or primary amine and separation of the epimers gave one stereoisomer with significantly more activity over the other, see **31** compared to **30** and **33** compared to **32**, Table 5. The more active isomer of the primary amine, compound **33**, exhibited activity approaching the cellular potency of the pyrazole ML-792 and showed good selectivity over both NAE and UAE. Methylation of the amine to the secondary or tertiary amine significantly reduced potency.

Substitution of the thiophene was also investigated. Chlorination or methylation at the 5-position were tolerated with the methylated compound **36** being more potent than the unsubstituted thiophene **29**. The polar and electron withdrawing cyano group at this position **38** was significantly less active, Table 6. Combining methylation of the thiophene and hydroxylation or amination of the benzylic center yielded highly potent compounds. The more active stereoisomers exhibiting only a 2- to 3-fold drop off in potency following washout and maintaining pathway inhibition below 50 nM at 8 h. Incorporating methylation at the benzylic position to give the tertiary alcohol or corresponding primary amine was well-tolerated and again demonstrated only a small drop off in potency between 0 and 8 h for the more active isomers in the washout assay, e.g. see **45**, Table 6.

The crystal structure of the adduct of the more active isomer of a tertiary alcohol analogue, compound **46**, in which the meta-chlorophenyl is replaced with 6-bromopyridyl, demonstrates the anticipated H-bond between the benzylic methylene hydroxyl group and serine 95, Figure 7. It also specifies the desired configuration of the benzylic center as *S*. Assuming a similar preferred orientation for the benzylic amino analogues, a rationale can be put forward to explain why methylation to the secondary or tertiary amine (compounds **34**, **35** in Table 5) is

https://dx.doi.org/10.1021/acs.jmedchem.0c01491
J. Med. Chem. 2021, 64, 2501−2520

Table 4. SAR Exploration of Alternative Benzyl Substituted Heterocycles

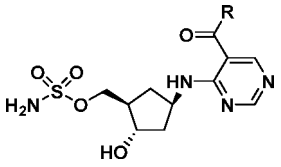

Compound	R	IC50 (nM)			SUMO IF
		SAE	NAE	UAE	IC50 (nM)
23	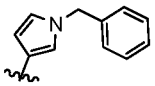	1.7	23	>1000	30
24	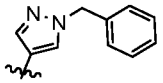	6.3	122	>1000	2940
25	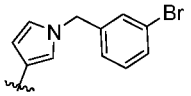	0.6	10	>1000	14
26	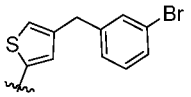	1.3	91	>1000	41
27	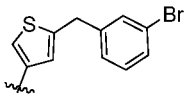	18	523	>1000	4930
28	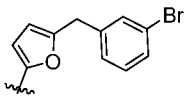	2.0	267	>1000	283

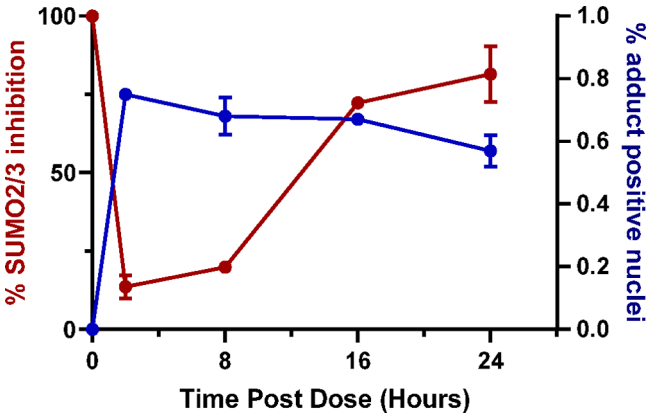

Figure 4. Pharmacodynamic effects of ML-792 in HCT-116 tumor bearing female NCr nude mice. Each data point represents the averaged value across $n = 3$ mice. Error bars = SEM. At $t = 0$, mice received a single SC injection of ML-792 at 150 mg/kg. Red line = percent nuclei staining positive for SUMO2/3 conjugation normalized to vehicle-treated animals. Blue line = percent nuclei staining positive for SUMO-ML-792 adduct.

less active, as the methyl group would either preclude access to this orientation or clash with the enzyme. The internal H-bond between the pyridine substituent and tertiary alcohol suggests that cyclization of the heteroatom to the pendant aryl group may be favored.

To investigate the effect of cyclization, we prepared both the isochromane and tetrahydroisoquinoline ring systems. The isochromane was indeed extremely potent and demonstrated prolonged cellular pathway inhibition; for example, ML-93 exhibited an IC_{50} of 15 nM at the 8 h time point in the SUMO IF assay. Similar to the open chain system, one isomer is highly preferred over the other, as can be seen by comparing ML-93 with **47**, Table 7. Meta-substitution had been shown to be preferred in the open benzylic analogues. The unmethylated thiophene analogue **50** and replacement of the methyl group with chloro, as in **48**, gave compounds of similar potency. Cyclization to the isochromane effectively fixes the orientation of the meta-substituents in two distinct areas of space. The 7-chloro-isochromane **50** was found to be significantly more active than the corresponding substitution at the 5-position as in **51**, Table 7. The matched pair of **48**, the 5-membered

https://dx.doi.org/10.1021/acs.jmedchem.0c01491
J. Med. Chem. 2021, 64, 2501−2520

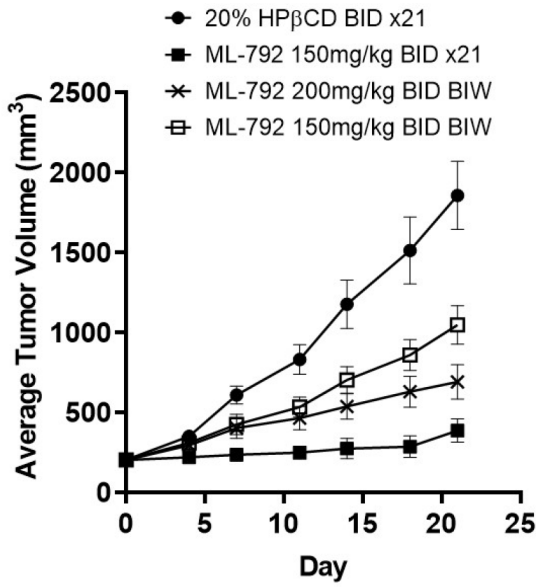

Figure 5. Antitumor efficacy of ML-792 at multiple dose/schedule regimens in Ncr/nude mice bearing HCT-116 tumor-bearing mice. (a) ML-792 was dosed subcutaneously at the dose and schedule indicated for each arm (n = 10 female NCr nude mice/arm) until the final treatment day on day 21. Schedules: BID x21 = twice per day for 21 days (days 1−21); BID BIW = twice per day/twice per week (days 1, 4, 8, 11, 15, 18, 21); BID 2on-5off = twice per day/twice per week on 2 consecutive days followed by 5 nondosing days (days 1, 2, 8, 9, 15, 16, 21).

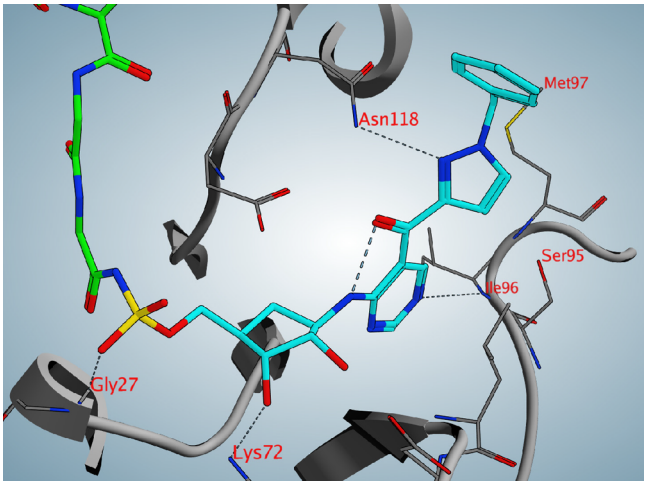

Figure 6. Structure of SUMO1-compound **2** adduct within SAE ATP binding domain. Carbon is shown in cyan (**2**), green (SUMO), or gray (SAE); nitrogen, blue; oxygen, red; and sulfur, yellow. Secondary structure of SAE is shown in gray. Hydrogen bonds are indicated by dashed lines. PDB accession code 6XOI.

dihydroisobenzofuran ring system **55**, was not well-tolerated with a significant loss of cell potency. The tetrahydroisoquinoline (THiQ) exemplified by TAK-981 also exhibited potent and prolonged cellular pathway inhibition with improved selectivity over NAE. Removal of the methyl or chloro-substituents (**58**, **59**) reduced cellular potency more so in the THiQ series than the isochromane series. Methylation of the THiQ nitrogen, as in **60**, also significantly reduced potency, and again, the 5-membered isoindoline ring system **61** suffered from reduced potency, e.g. comparing **57** with **61**, Table 7. A crystal structure of the SUMO−compound **49** adduct confirmed the configuration of the isochromane, and the isochromane oxygen and ser-95 are within contact distance to form an H-bond, Figure 8. The corresponding residues to Ser-95 are Lys-147 and Arg-551 in NAE and UAE, respectively, which may explain the particularly high selectivity for the basic amino-containing compounds such as TAK-981.[18,34] The H-bonding to ser-95 may favor orientation of the isochromane and THiQ groups to form hydrophobic interactions with the enzyme and contribute to prolong binding of the adduct. The residence time of the adduct in the enzyme is thought to be particularly important for cellular potency as released adduct may be susceptible to cleavage by cellular endoproteases such as SUMO specific endoproteases (SENPs).[19,35]

Having established durable pathway inhibition in cells, we investigated whether this translated into a prolonged response in

Table 5. SAR Exploration of Benzylic Substitution on Thiophene

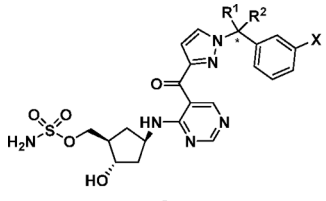

a

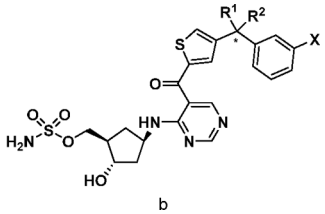

b

compound	structure	R^1	R^2	X	IC_{50} (nM) SAE	NAE	UAE	SUMO IF IC_{50} (nM) (washout 0, 8 h)[a]
ML-792	a	H	H	Br	0.4	228	>1000	10 (25, 246)
26	b	H	H	Br	1.3	91	>1000	41 (52, 650)
29	b	H	H	Cl	1.0	64	>1000	68 (142, 2060)
30[b]	b	OH	H	Cl	1.0	114	>1000	660 (1210, >10 000)
31[b]	b	H	OH	Cl	0.2	216	>1000	55 (43, 955)
32[b]	b	NH_2	H	Cl	1.5	328	>1000	1030 (−, −)
33[b]	b	H	NH_2	Cl	0.7	>1000	>1000	50 (83, 499)
34[b]	b	NHMe	H	Cl	3.7	956	>1000	436
35[b]	b	NMe_2	H	Cl	25	>1000	>1000	4170

[a]IC_{50} immediately following washout of compound, 0 h, or after 8 h. [b]Single diastereomer, undefined configuration. [c]Mixture of diastereomers.

https://dx.doi.org/10.1021/acs.jmedchem.0c01491
J. Med. Chem. 2021, 64, 2501−2520

Table 6. SAR Exploration Thiophene Substitution

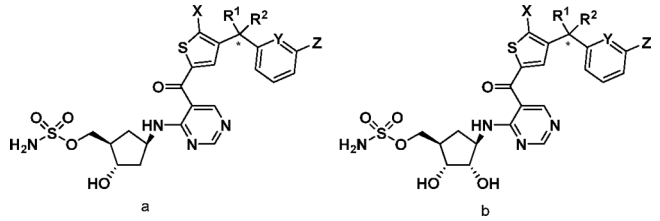

a b

compound	structure	R^1/R^2	X	Y	Z	IC50 (nM) SAE	NAE	UAE	SUMO IF IC_{50} (nM) washout (0, 8 h)
36	a	H/H	CH_3	CH	Cl	1.2	32	>1000	19 (66, 403)
37	a	H/H	Cl	CH	Cl	3.6	681	>1000	108 (184, 1400)
38	a	H/H	CN	CH	Cl	19	>1000	>1000	6260
39	a	OH[a]/H	CH_3	CH	Cl	0.3	64	>1000	6 (8, 21)
40	a	OH[a]/H	Cl	CH	Cl	0.3	341	>1000	9 (17, 70)
41	a	NH_2[a]/H	CH_3	CH	Cl	0.2	235	>1000	16 (19, 38)
42	a	NH_2[a]/H	Cl	CH	Cl	0.4	861	>1000	10 (17, 39)
43	a	OH[a]/H	Cl	N	Cl	0.2	340	>1000	14 (16, 142)
44	a	OH[a]/CH_3	H	CH	Cl	0.2	343	>1000	12 (19, 233)
45	a	NH_2[a]/CH_3	H	CH	Cl	0.3	>1000	>1000	16 (29, 101)
46	b	OH[b]/CH_3	H	N	Br	0.1	31	616	47 (251, 361)

[a]More active diastereomer at this center. [b]*S*-Configuration at this center.

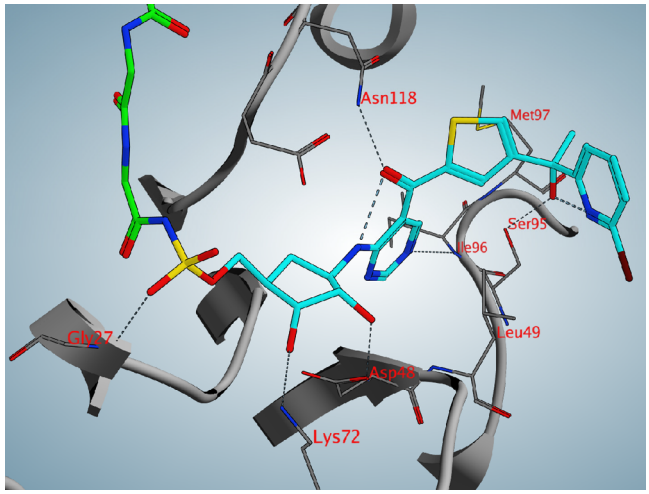

Figure 7. Structure of SUMO1-compound **46** adduct bound to SAE. Carbon is shown in cyan for compound **46**, green (SUMO), or gray (SAE); nitrogen, blue; oxygen, red; bromide, dark red; and sulfur, yellow. Secondary structure of SAE is shown in gray. Hydrogen bonds are indicated by dashed lines. PDB accession code 6XOG.

a solid tumor xenograft (HCT-116; colorectal carcinoma) and a hematological tumor xenograft (OCI-Ly10; DLBCL) model. A PD time course for the isochromane ML-93 and the corresponding THiQ TAK-981 compared to the initial lead ML-792 in HCT-116 is shown in Figure 9a and in OCI-Ly10 is shown in Figure 9b. In HCT-116, the depletion of SUMO-conjugated proteins is much more sustained for ML-93 and TAK-981 than for ML-792. Even with lower dose of ML-93 (50 mg/kg) and TAK-981 (50 mg/kg in HCT116 and 25 mg/kg in LY10), we observed less than 25% recovery through 16 h. Consistently, similar improvement in the durability of the SUMO−inhibitor adduct was observed for ML-93 and TAK-981 compared to ML-792 in the HCT-116 model, Figure 10a and OCI-Ly10 model, Figure 10b. The adduct to SAE enzyme ratio as determined by mass spectrometry, remains close to unity even at 16 h for TAK-981, Figure 10a. All three compounds exhibit similar relatively rapid decrease in plasma concentration to below detection by 8 h in the HCT-116 tumor bearing mice, Figure 11a and in the OCI-Ly10 tumor bearing mice, Figure 11b. Compound ML-93 and TAK-981 showed similar potency and viability effects in the HCT116 cells cultured in vitro, as previously observed for compound ML-792, Table 8.[33] An efficacy study in HCT116 model demonstrated equivalent tumor growth inhibition (tumor stasis, Figure 12a) at much lower weekly dosage for ML-93 (50 mg/kg, QDX21, total weekly dose = 350 mg/kg) and TAK-981 (50 mg/kg QDX3/week, total weekly dose = 150 mg/kg) compared to ML-792 (150 mg/kg, BID, total weekly dose = 2100 mg/kg), Figure 12b. Similar results and tumor regression were observed in the OCI-Ly10 model, Figure 12c, d. This is consistent with the Ly10 cells being intrinsically more sensitive than HCT-116 for example a cellular viability EC_{50} for TAK-981 of 4 and 63 nM in LY10 and HCT-116, respectively, Table 8.

The ADME properties of ML-93 and TAK-981 are similar to those of ML-792, exhibiting high extraction ratios in liver S9 subcellular fractions, indicating these compounds are subject to a relatively high degree of metabolism in the liver, Table 8. The results from the permeability assay using Caco-2 cells showed high efflux ratios of >16, and the resulting low apparent permeability for all three compounds indicate these compounds are substrates of efflux transporters, Table 8. The PK of the compounds in rat are similar, exhibiting high blood to plasma ratios, relatively short half-lives, and low exposures following an oral administration due to relatively poor oral bioavailability, Table 9. The high blood to plasma partitioning may be attributed to reversible binding to carbonic anhydrase (CA), Table 8, which present in high levels in red blood cells, through the sulfamate group.[36,37] The PK profiles in blood and plasma exhibited parallel terminal phases with comparable half-lives in both matrixes, indicting the high blood to plasma partitioning of these compounds is considered to be in rapid equilibrium.

Even though these compounds showed a relatively short half-life, both ML-93 and Tak-981 demonstrated a durable PD

https://dx.doi.org/10.1021/acs.jmedchem.0c01491
J. Med. Chem. 2021, 64, 2501−2520

Table 7. SAR Exploration of Isochromane and Tetrahydroisoquinoline Substituents[a]

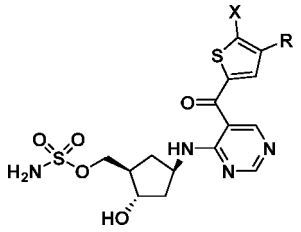

Compound	R	X	IC50 (nM)			SUMO IF IC50 (nM) Washout (0, 8h)
			SAE	NAE	UAE	
ML-93	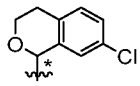	CH_3	0.4	386	>1000	3 (7, 15)
47	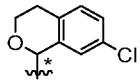	CH_3	11	87	>1000	3880
48	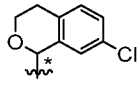	Cl	1.0	>1000	>1000	8 (10, 14)
49	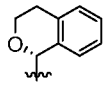	H	0.4	198	>1000	4 (5, 39)
50	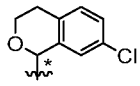	H	0.5	450	>1000	8 (7, 22)
51	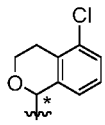	H	1.7	265	>1000	76
52	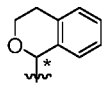	CH_3	0.3	102	>1000	6 (4, 14)
53	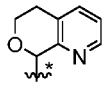	CH_3	0.2	507	>1000	-- (19, 64)

https://dx.doi.org/10.1021/acs.jmedchem.0c01491
J. Med. Chem. 2021, 64, 2501−2520

Table 7. continued

54	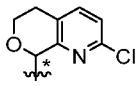	CH_3	0.1	203	>1000	20 (18, 89)
55	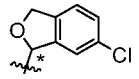	Cl	3.0	>1000	>1000	163
TAK-981	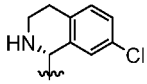	CH_3	1.0	960	>1000	15 (32, 46)
56	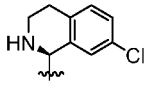	CH_3	30	554	>1000	399
57	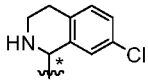	Cl	0.4	>1000	>1000	7 (9, 17)
58	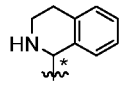	H	1.0	>1000	>1000	78 (365, 503)
59	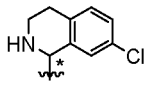	H	0.8	>1000	>1000	27 (167, 142)
60	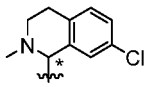	H	2.5	>1000	>1000	638
61	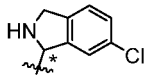	Cl	1.6	>1000	>1000	312

[a]An asterisk indicates a more active diastereomer, undefined configuration.

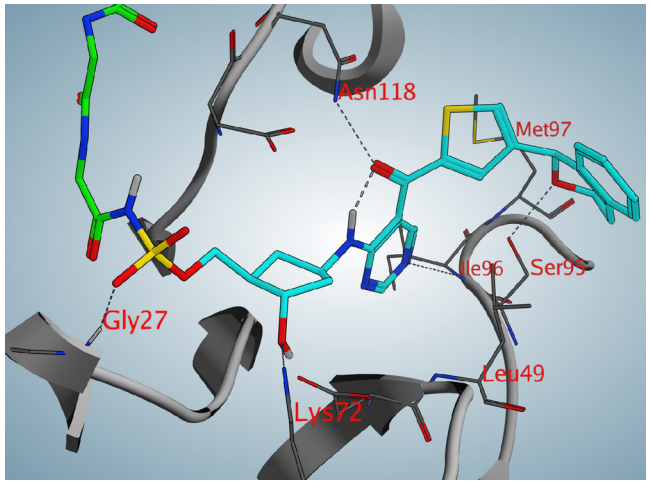

Figure 8. Crystal structure of SAE with SUMO1-compound **49** adduct. Carbon is shown in cyan, **49**, green (SUMO), or gray (SAE); nitrogen, blue; oxygen, red; and sulfur, yellow. Secondary structure of SAE is shown in gray. Hydrogen bonds are indicated by dashed lines. PDB accession code 6XOH.

response and robust efficacy, including on intermittent dosing schedules, at greatly reduced dose compared to the initial lead ML-792. In light of this disconnect between PK and PD, driven by the tight binding nature of the inhibitor adduct to the enzyme, the team saw no requirement for improved exposure kinetics as a criterion for development as a parentally administered agent. With this in mind, the equilibrium solubility of TAK-981 compared to ML-93 was substantially higher at mildly acidic pH due to the presence of the basic THiQ system (pK_a 7.5, Table 8). In the presence of hydroxypropylcyclodextrin (hpβcd) excipient, the equilibrium solubility at approximately 20 mg/mL was acceptable for development as an i.v. formulation.

ML-93 has recently been investigated in pancreatic ductal carcinoma (PDAC), providing evidence of sensitivity to SAE inhibition and activation of MYC.[14] Exploration of the activity of TAK-981 in mouse models and primary cell explants revealed upregulation of Type I IFN signaling in immune cells and Type I IFN dependent activation of innate immune cells, including macrophages, NK cells and dendritic cells, as well as T cells.[38] In mouse syngeneic tumor models, TAK-981 was shown to promote an innate immune response capable of bridging to an adaptive antitumor immune response, representing a novel and mechanistically differentiated strategy for stimulating Type I

https://dx.doi.org/10.1021/acs.jmedchem.0c01491
J. Med. Chem. 2021, 64, 2501−2520

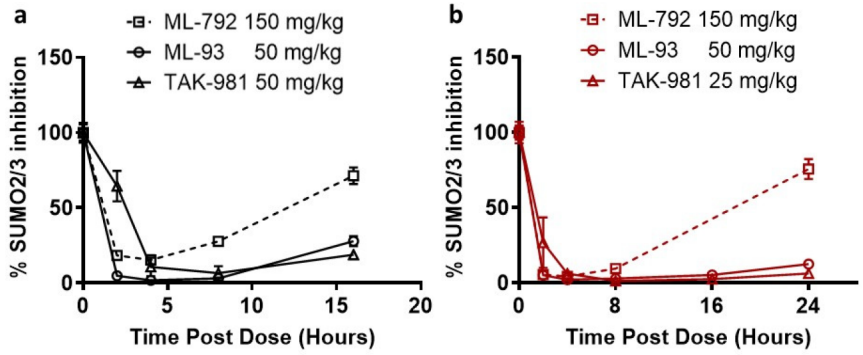

Figure 9. Reduction of SUMO2/3 conjugation in xenograft tumors following IV administration of SUMOylation inhibitors. Each data point represents the averaged value across n = 3 female Ncr nude mice. Error bars = SEM. Percent SUMO2/3 inhibition following compound administration represented as percent nuclei staining positive by IHC for SUMO2/3 conjugates/total nuclei normalized to vehicle-treated animals (time = 0 h). SUMOylation inhibitors were administered at time = 0. ML-792 was dosed at 150 mg/kg SC (dashed line/open square). ML-93 was dosed at 50 mg/kg IV (solid line/open circle). TAK-981 was dosed at 50 mg/kg IV (solid line/open triangle). (a) Reduction of SUMO2/3 conjugation at 2, 4, 8, and 16 h postinjection in HCT-116 tumors. (b) Reduction of SUMO2/3 conjugation at 2, 4, 8, 16, and 24 h postinjection in OCI-Ly10 tumors.

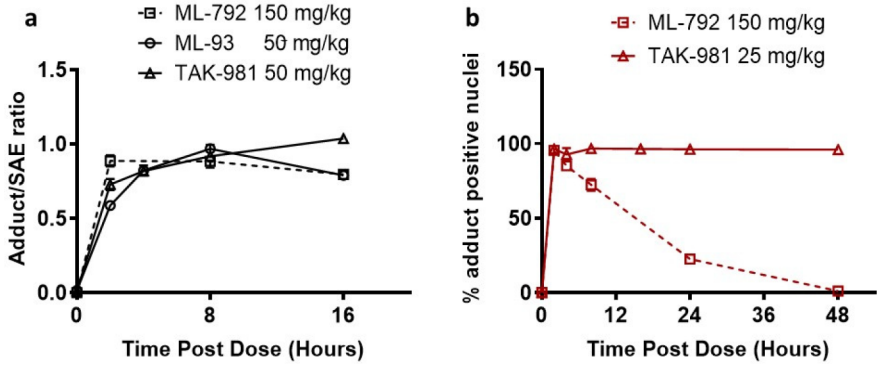

Figure 10. Gain of SUMO−compound adduct in xenograft tumors following IV administration of SUMOylation inhibitors. Adduct formation in xenograft tumors following compound administration. Each data point represents the averaged value across n = 3 female Ncr nude mice. Error bars = SEM. (a) Single-dose ML-792 at 150 mg/kg IV (dashed line/open square), ML-93 at 50 mg/kg IV (solid line/open circle) or TAK-981 (solid line/open triangle) was administered to Ncr/nude mice bearing HCT116 tumors. Tumors were harvested 2, 4, 8, and 16 h post IV injection. Adduct/SAE ratio = quantity SUMO−compound adduct/quantity total SAE enzyme as measured by mass spectrometry. (b) Single-dose ML-792 at 150 mg/kg IV (dashed line/open square) or TAK-981 at 25 mg/kg IV (solid line/open triangle) was administered to CB17 SCID mice bearing OCI-Ly10 tumors. Tumors were harvested 2, 4, 8, 24, and 48 h post IV injection. Percent nuclei staining positive for adduct was measured by IHC.

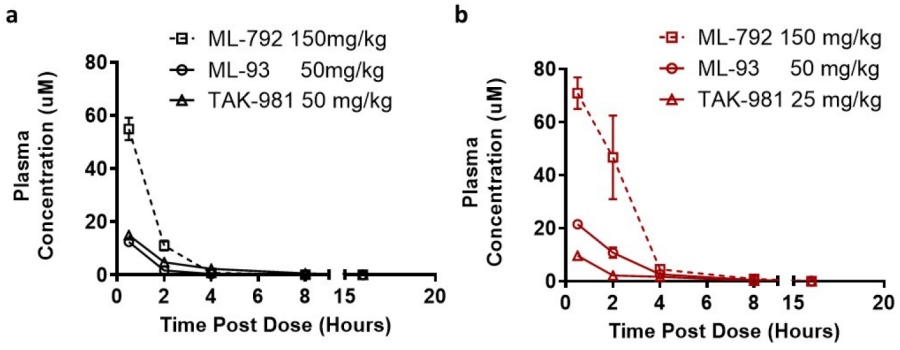

Figure 11. Plasma exposure following single-dose IV administration. Plasma collected at indicated time-point postinjection by cardiac blood collection followed by centrifugation. Each data point represents the averaged value across n = 3 female Ncr nude mice. Error bars = SEM. (a) Single-dose injection at t = 0 delivered to Ncr/nude mice bearing HCT-116 tumors with the indicated compounds and dosages or (b) single-dose injection at t = 0 delivered to CB17 SCID mice bearing OCI-Ly10 tumors with the indicated compounds and dosages. Plasma samples were collected at 0.5, 2, 4, 8, and 16 h postinjection via cardiac blood collection followed by centrifugation.

IFN signaling and antitumor immune responses.[39] The activity of TAK-981 is currently being assessed in Ph1 clinical trials in adult patients with solid tumors and lymphomas (NCT03648372, NCT04074330, and NCT04381650).

Chemistry. The synthetic route used to synthesize the analogues described in Tables 1 and 2 is detailed in Scheme 2. Benzylation of pyrazol-3-carbaldehyde provided the desired N1-benzyl pyrazole in a highly regiospecific manner. Lithium halogen metal exchange of 4-chloro-5-iodopyrimidine followed

https://dx.doi.org/10.1021/acs.jmedchem.0c01491
J. Med. Chem. 2021, 64, 2501−2520

Table 8. Profiles of ML-792, ML-93, and TAK-981

compound	LogD pH 7.4	pK_a	CaCo2 A-B, B-A 10^{-6} cm/s	Int CL[a] E_h human, rat	solubility[b] μg/mL	CA[c] 1, 2 IC_{50} μM pH 3.5	cell viability HCT116, LY10 EC_{50} μM
ML-792	2.6	3.6, 8.8	1.2, 64	0.7, 0.8		0.05, 0.01	0.090, 0.055
ML-93	1.9	3.5, 8.9	4.0, 64	0.9, 0.9	100	0.05, 0.01	0.110, 0.004
TAK-981	2.1	3.6, 7.5, 8.8	0.3, 46	0.8, 0.9	20 000	0.09, 0.02	0.063, 0.004

[a]Intrinsic clearance (Int CL) expressed as predicted hepatic extraction ratio E_h. [b]Determined at 24 h in the presence of 10% hpβcd. [c]Carbonic anhydrase, isoform 1 and 2.

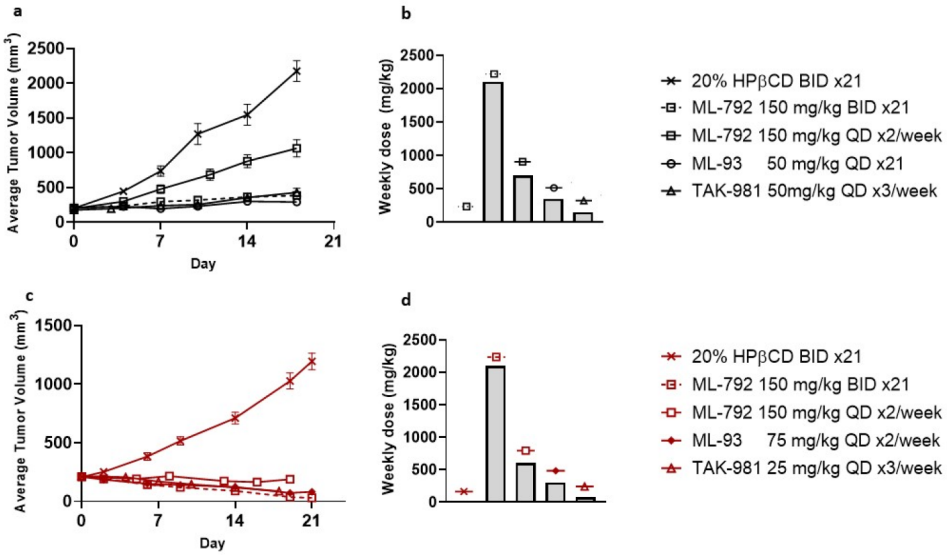

Figure 12. Antitumor activity versus total weekly dosage in human xenograft cancer models. Line graphs = average tumor volumes over time. Error bars = SEM. Mice were randomized into groups on Day 0. Treatment started on Day 1. Tumor volume measurements were taken twice per week. Bar graphs = total weekly dose for each treatment arm. (a) Female Ncr/nude mice bearing HCT-116 tumors (~200 mm^3 volume) were randomized into 5 groups (n = 8/group). Treatment started on Day 1. Tumor volumes were measured twice per week. Error bars represent SEM. (b) Total weekly dose administered to mice in each arm of the HCT-116 efficacy study (panel a) is calculated, demonstrating reduced compound required to achieve efficacy with TAK-981. (c) Female CB17 SCID mice bearing OCI-Ly10 tumors (~200 mm^3 volume) were randomized into 5 groups (n = 8/group). Treatment started on Day 1. Tumor volumes were measured twice per week. Error bars represent SEM. (d) Total weekly dose administered to mice in each arm of the OCI-Ly10 efficacy study (panel c) is calculated, demonstrating reduced compound required to achieve efficacy with TAK-981. Dosing schedules: BID x21 = twice-per-day (Days 1−21); QD x2/week = twice per week (Days 1, 4, 8, 11, 15, 18); QD x21 = once-per-day (Days 1−21); QD x3/week = thrice-per-week (Days 1−21); QD x3/week = three consecutive dosing days followed by four nondosing days (Days 1, 2, 3, 8, 9, 10, 15, 16, 17).

Table 9. In Vivo Profiles of ML-792, ML-93, and TAK-981[a]

	PK rat					
	i.v. 1 mpk				p.o. 10 mpk	
compound	AUC (μM·h) blood, plasma	CL (L/h/kg) blood, plasma	V_{ss} (L/kg) blood, plasma	$T_{1/2}$ (h) blood, plasma	AUC (μM·h) blood, plasma	%F blood, plasma
ML-792	19.1, 0.4	0.1, 5.1	0.1, 5.1	1.2, 0.9	10.8, 0.1	6.9, 7.1
ML-93	12.5, 0.3	0.1, 5.2	0.2, 5.0	4.0, 1.5	24.1, 0.6	19, 18
TAK-981	31.2, 0.5	0.1, 3.7	0.2, 8.5	2.6, 2.1	32.0, 0.3	10.0, 7.3

[a]N = 3 animals, rat. mpk = mg per kg.

by addition of the aldehyde afforded the benzylic alcohol, which was oxidized with MnO_2 to provide an intermediate chloropyrimidine ketone (**I-3**). Displacement of the chloride with the appropriately substituted amino cyclopentane in the presence of base yielded intermediates which were further elaborated to final products by protecting group manipulation and sulfamation.

Scheme 3 details the synthetic route used to synthesize the analogues described in Table 3. The appropriately substituted N-Boc pyrazole (**I-25**) intermediate was prepared as described in Scheme 2. Substitution of the pyrazole was performed in an array format by one of two methods, Scheme 3. Either the primary alcohol was initially sulfamated, followed by N-Boc deprotection to provide an intermediate that was selectively *N*-alkylated through parallel array, or alternatively, the Boc group was removed first to provide an intermediate that was subsequently *N*-alkylated followed by sulfamation.

Schemes 4 and 5 detail the synthetic route used to prepare the benzylic alcohol or benzylic amine analogues described in Tables 5 and 6. Metal halogen exchange of the bromothiophene and reaction either with the appropriate benzaldehyde or benzylic sulfonyl imine gave the secondary alcohol or sulfonyl amine. Protecting group manipulation gave the thiophene aldehyde intermediate suitable for reaction with 4-chloro-5-iodopyrimidine, and subsequent elaboration analogous to that shown in Scheme 2 gave the target compound, Scheme 4. The tertiary alcohols were prepared in a similar manner starting from the appropriate acetophenone. The alpha-methyl amines were prepared through oxidation of the secondary alcohol to the ketone, formation of the sulfonylimine, followed by reaction with methyllithium, Scheme 5. Separation of the epimers was

https://dx.doi.org/10.1021/acs.jmedchem.0c01491
J. Med. Chem. 2021, 64, 2501−2520

Scheme 2. Synthesis of Pyrazolo Analogues Described in Tables 1 and 2

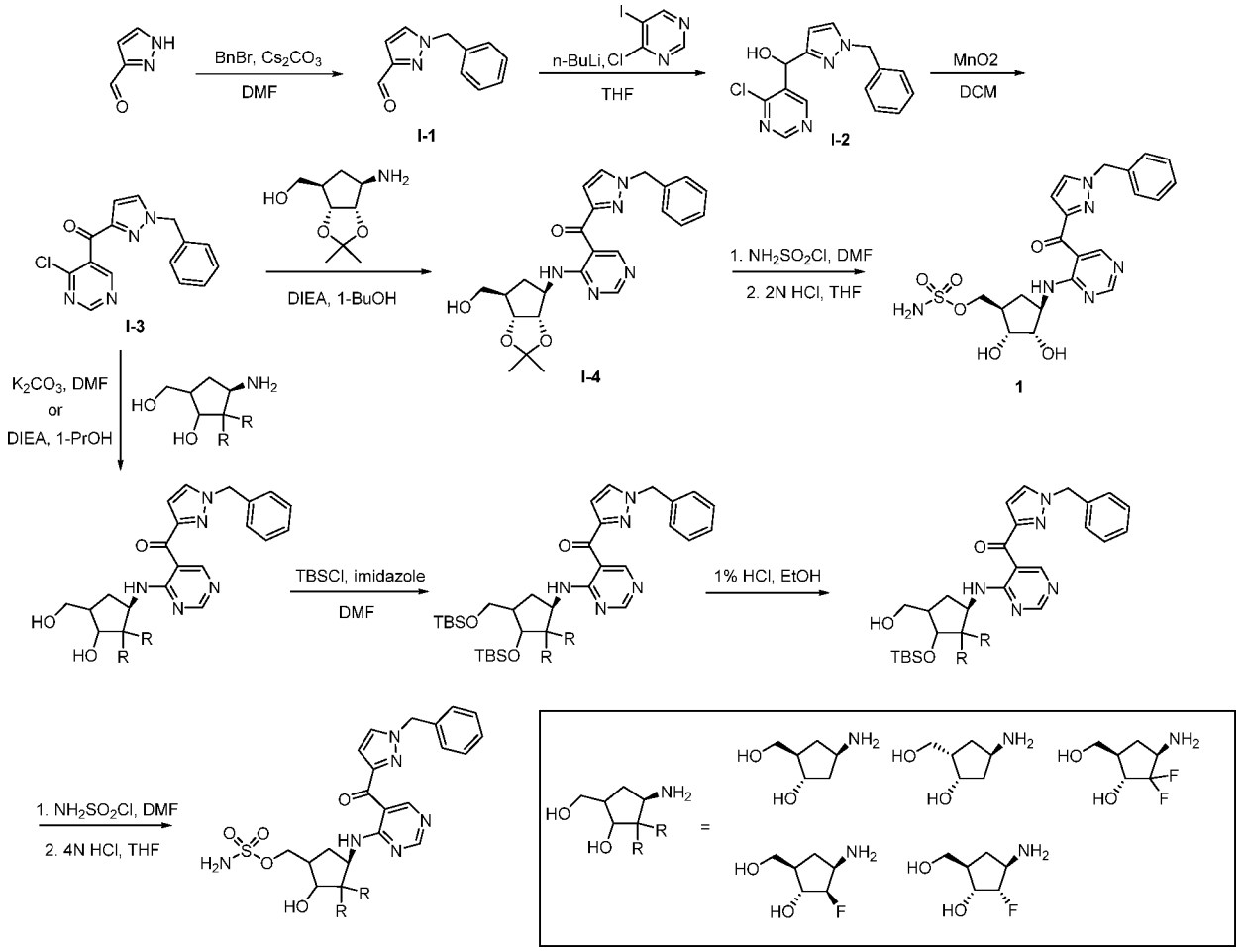

Scheme 3. Synthetic Routes Employed for Pyrazolo-Substitution by Parallel Array

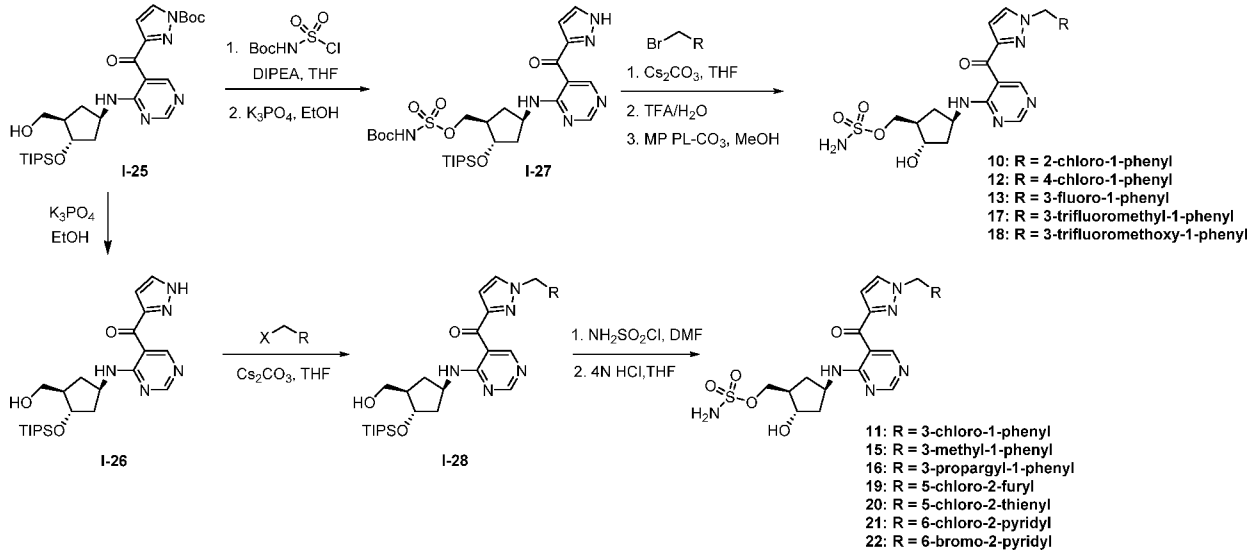

achieved through SFC or prep HPLC on the final sulfamated compounds.

Scheme 6 details the synthetic route used to prepare the isochromane and tetrahydroisoquinoline analogues described in Table 7. Metal halogen exchange of the bromothiophene and reaction with a benzaldehyde derivatized at the ortho position with an appropriately protected alcohol. Treatment with acid deprotected the primary alcohol and facilitated cyclization to give the isochromane (**I-107**). The thiophene aldehyde was then progressed to the final compounds by an analogous route to Scheme 2.

https://dx.doi.org/10.1021/acs.jmedchem.0c01491
J. Med. Chem. 2021, 64, 2501−2520

Scheme 4. Synthesis of Key Intermediates for Benzylic Alcohol and Benzylic Amines Described in Tables 5 and 6

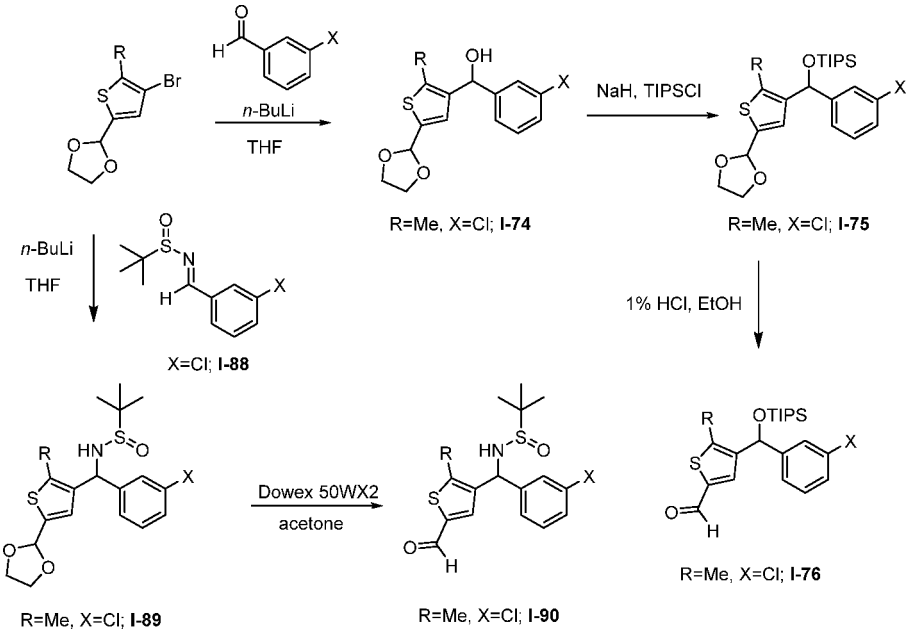

Scheme 5. Synthesis of Key Intermediates for Alpha-Methyl Benzyl Amines

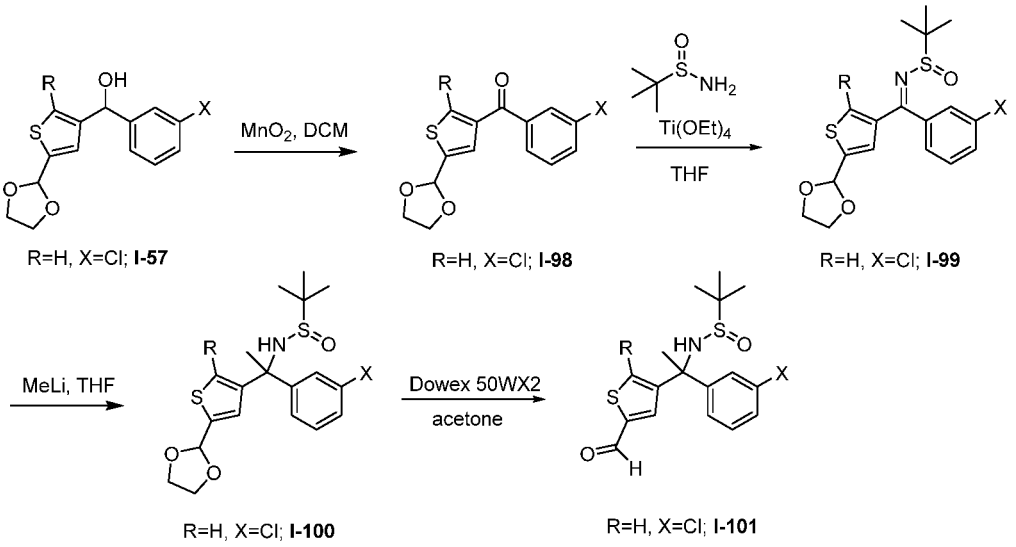

The tetrahydroisoquinoline analogues (**I-117**) were prepared in a similar fashion by reaction with the appropriate dihydroisoquinoline and prosecution to the target compound. Separation of the epimers was achieved through SFC or prep HPLC on the final sulfamated compounds. The configuration of the more active isomer at the THiQ center was designated as *R* from a small molecule crystal structure of a late stage, presulfamation, synthetic intermediate on route to TAK-981. This was subsequently confirmed through a micro-ED crystal structure of TAK-981, Figure 13.

CONCLUSION

In conclusion, a series of small molecule mechanism-based inhibitors of SAE have been identified and described in this report. These compounds act through a substrate assisted mechanism and demonstrate robust and selective inhibition of SAE and the SUMO pathway in cells and in vivo models. A distinct allosteric covalent inhibitor approach demonstrating in vivo activity has also recently been described.[40,41] An iterative medicinal chemistry program optimized a nonselective compound, identified from a scaffold hopping exercise, into inhibitors that form tight binding SUMO−inhibitor adducts that exhibit extended duration of target and pathway inhibition. This work has culminated in the identification of TAK-981 which has entered clinical trials in metastatic solid tumors in combination with pembrolizumab, and in Non-Hodgkin's lymphoma in combination with rituximab (NCT03648372, NCT04074330, and NCT04381650).

EXPERIMENTAL SECTION

All animal studies were conducted under the approval of the Takeda Oncology Institutional Animal Care and Use Committee and complied with all relevant ethical regulations. Mice were maintained in a specific pathogen-free facility in accordance with American Association for

https://dx.doi.org/10.1021/acs.jmedchem.0c01491
J. Med. Chem. 2021, 64, 2501−2520

Scheme 6. Synthesis of Key Intermediates for Isochromane and Tetrahydroisoquinoline Compounds Described in Table 7

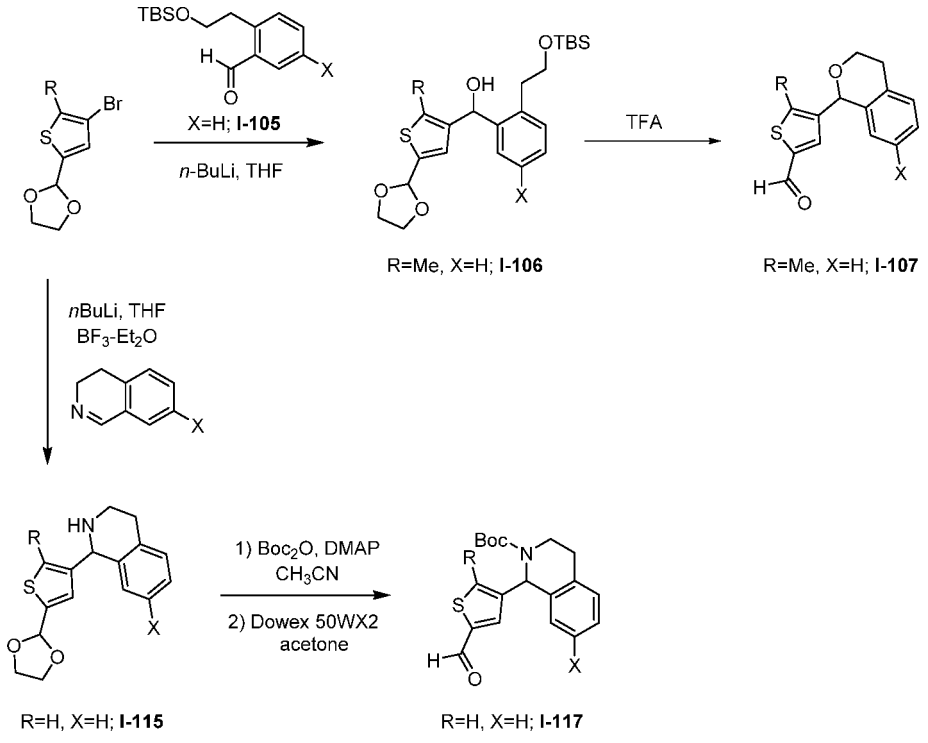

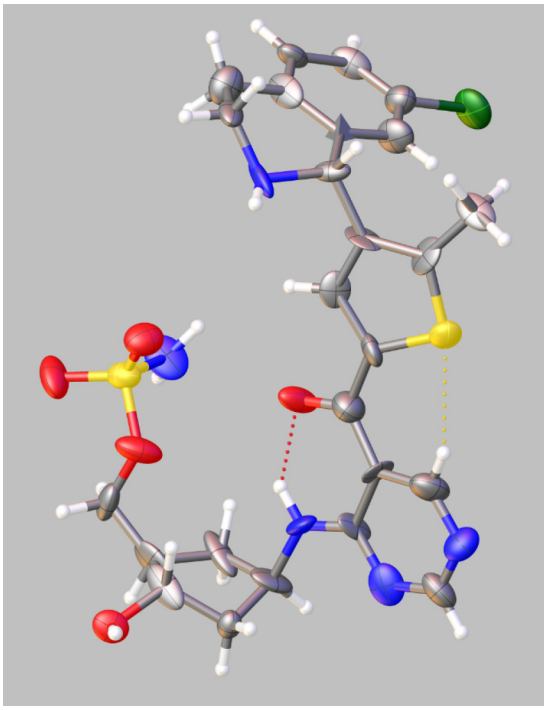

Figure 13. Crystal structure of TAK-981 solved by microelectron diffraction (microED) technique. Carbon is shown in gray; hydrogen, white; nitrogen, blue; oxygen, red; sulfur, yellow; chlorine, green. CCD accession code CCDC 2013738.

Laboratory Animal Science guidelines. See Supporting Information for in vivo protocols.

Chemistry. NMR spectra were recorded in the solvent reported on a 400 MHz Bruker spectrometer using residual solvent peaks as the reference. Compound purity was determined by analysis of the diode array UV trace of an LC-MS spectrum using the following procedure: compounds were dissolved in DMSO, methanol, or acetonitrile, and the solutions were analyzed using a Hewlett-Packard HP1100 or Agilent 1100 Series LC system connected to a Micromass mass spectrometer using reverse phase C18 columns. One of two gradients was used to elute the compounds: either a formic acid (FA) gradient (acetonitrile containing 0−100% 0.1% formic acid in water) or an ammonium acetate (AA) gradient (acetonitrile containing 0−100% 10 mM ammonium acetate in water). All compounds were determined to be >95% pure unless otherwise noted.

Synthesis of 2. *Step 1:1-Benzyl-1H-pyrazole-3-carbaldehyde (I-1).* A 100 mL round-bottom flask was charged with 1-pyrazole-3-carbaldehyde (250 mg, 2.60 mmol), Cs_2CO_3 (2.12 g, 6.50 mmol), and DMF (10 mL). To the suspension was added benzyl bromide (0.33 mL, 2.70 mmol), and the reaction was stirred for 1 h. The reaction mixture was poured into water (50 mL), and the mixture was extracted with EtOAc (50 mL) three times. The combined organic layers were washed with brine, dried over Na_2SO_4, filtered, and concentrated in vacuo. The residue was purified on silica gel to provide I-1 (372 mg, 77%). ^{1}H NMR ($CDCl_3$) δ 10.01−9.98 (m, 1H), 7.42 (d, 1H, J = 2.3 Hz), 7.41−7.32 (m, 3H), 7.28−7.23 (m, 2H), 6.82 (d, 1H, J = 2.4 Hz), 5.40 (s, 2H).

Step 2: (1-Benzyl-1H-pyrazol-3-yl)(4-chloropyrimidin-5-yl)-methanol (I-2). 4-Chloro-5-iodopyrimidine (300 mg, 1.25 mmol) was weighed into a 100 mL 2-necked round-bottom flask, and the flask was purged with argon. This starting material was dissolved in THF (10 mL), and the solution was cooled to −78 °C. To the solution was added *n*-BuLi (2.50 M in hexane; 1.0 mL, 2.5 mmol) at −78 °C, and then the mixture was stirred for 30 min. To this mixture was added dropwise a solution of 1-benzyl-1*H*-pyrazole-3-carbaldehyde (211 mg, 1.1 mmol) in THF (4 mL), and the resulting mixture was stirred for 30 min. The reaction was quenched by addition of saturated NH_4Cl (50 mL) and extracted with EtOAc (50 mL) four times. The combined organic layers were washed with brine, dried over Na_2SO_4, filtered, and concentrated in vacuo. The residue was purified on silica gel to provide **I-2** (304 mg, 85%) as a light-yellow oil. LCMS (FA): m/z = 301.4 (M+H).

Step 3: (1-Benzyl-1H-pyrazol-3-yl)(4-chloropyrimidin-5-yl)-methanone (I-3). To a solution of (1-benzyl-1*H*-pyrazol-3-yl)(4-chloropyrimidin-5-yl)methanol (285 mg, 0.95 mmol) in DCM (10 mL) was added MnO_2 (0.82 g, 9.5 mmol), and the mixture was stirred for 15 h at rt. The reaction was filtered through a pad of Celite, and the residual solid was washed with DCM several times. The filtrate was

https://dx.doi.org/10.1021/acs.jmedchem.0c01491
J. Med. Chem. 2021, 64, 2501−2520

concentrated in vacuo, and the residue was purified on silica gel to give **I-3** (257 mg, 91%) as a colorless solid. ^{1}H NMR ($CDCl_3$) δ 9.09 (s, 1H) 8.90 (s, 1H) 7.45 (d, 1H, J = 2.5 Hz) 7.32−7.41 (m, 3H) 7.22 (m, 2H) 7.02 (d, 1H, J = 2.5 Hz) 5.33 (s, 2H); LCMS (FA): m/z = 299.4 (M+H).

*Step 4: (1-Benzyl-1H-pyrazol-3-yl)[4-({(1R,3R,4S)-3-(hydroxymethyl)-4-[(triisopropylsilyl)oxy]cyclopentyl}amino)pyrimidin-5-yl]methanone (**I-9**).* To a solution of {(1*R*,2*S*,4*R*)-4-amino-2-[(triisopropylsilyl)oxy]cyclopentyl}methanol-TFA (**I-8**, 1.04 g, 2.58 mmol) in DMF (20 mL) was added K_2CO_3 (1.1 g, 7.7 mmol) followed by (1-benzyl-1*H*-pyrazol-3-yl)(4-chloropyrimidin-5-yl)methanone (**I-3**, 0.85 g, 2.8 mmol) at rt, and the mixture was stirred for 13 h. The reaction was then concentrated in vacuo. To the residue was added water (100 mL), and the mixture was extracted with EtOAc (100 mL) three times. The combined organic layers were washed with brine, dried over Na_2SO_4, filtered, and concentrated in vacuo. The residue was purified on silica gel to give **I-9** (1.08 g, 75%) as a colorless oil. ^{1}H NMR ($CDCl_3$) δ 9.66 (s, 1H), 9.25 (br d, 1H, J = 7.3 Hz), 8.64 (s, 1H), 7.42 (d, 1H, J = 2.5 Hz), 7.40−7.31 (m, 3H), 7.28−7.23 (m, 2H), 6.89 (d, 1H, J = 2.3 Hz), 5.39 (s, 2H), 4.87−4.76 (m, 1H), 4.32 (q, 1H, J = 4.7 Hz), 3.70 (t, 2H, J = 5.4 Hz), 2.50 (td, 1H, J = 13.1, 8.0 Hz), 2.24−2.14 (m, 2H), 1.92−1.81 (m, 2H), 1.32 (td, 1H, J = 13.1, 8.1 Hz), 1.11−1.03 (m, 21H). LCMS (FA): m/z = 550.7 (M+H).

*Step 5: [(1R,2S,4R)-4-({5-[(1-Benzyl-1H-pyrazol-3-yl)carbonyl]-pyrimidin-4-yl}amino)-2-hydroxycyclopentyl]methyl sulfamate (**2**).* To a solution of (1-benzyl-1*H*-pyrazol-3-yl)[4-({(1*R*,3*R*,4*S*)-3-(hydroxymethyl)-4-[(triisopropylsilyl)oxy]cyclopentyl}amino)pyrimidin-5-yl]methanone (1.0 g, 1.8 mmol) in DMF (30 mL) was added chlorosulfonamide (650 mg, 5.6 mmol) at rt, and the mixture was stirred for 20 min. The reaction was quenched by addition of saturated $NaHCO_3$ (100 mL) and water (50 mL). The mixture was extracted with EtOAc (150 mL) three times, and the combined organic layers were dried over Na_2SO_4, filtered, and concentrated in vacuo. The residue was purified on silica gel to give the sulfamate intermediate [(0.91 g, 80%); LCMS (FA): m/z = 629.7 (M+H)] which was then dissolved in THF (20 mL) and HCl (4 M in water; 20 mL, 80 mmol) was added at rt. This mixture was stirred for 1 h and then quenched by addition of saturated $NaHCO_3$ (150 mL) and extracted with EtOAc (200 mL) four times. The combined organic layers were dried over Na_2SO_4, filtered, and concentrated in vacuo. To the residue was added DCM and the resulting suspension was filtered through a glass frit funnel, and the residual solid was washed with DCM twice. The filtrate was concentrated in vacuo, and the residue was purified on silica gel. The purification product and solid from filtration were combined to give **2** (652 mg, 95%) as a colorless solid. ^{1}H NMR (DMSO-d_6) δ 9.46 (s, 1H), 9.00 (d, 1H, J = 7.5 Hz), 8.62 (s, 1H), 8.07 (d, 1H, J = 2.4 Hz), 7.45 (s, 2H), 7.41−7.25 (m, 5H), 6.90 (d, 1H, J = 2.4 Hz), 5.50 (s, 2H), 4.92 (d, 1H, J = 4.6 Hz), 4.76−4.64 (m, 1H), 4.10 (dd, 1H, J = 9.7, 5.9 Hz), 4.01−3.92 (m, 2H), 2.41−2.30 (m, 1H), 2.19−2.07 (m, 1H), 2.00 (ddd, 1H, J = 11.7, 7.7, 3.8 Hz), 1.83−1.72 (m, 1H), 1.28 (dt, 1H, J = 12.9, 9.2 Hz). LCMS (FA): m/z = 473.5 (M+H). HRMS m/z $[M + H]^+$ calcd for $C_{21}H_{25}N_6O_5S$ 473.1607, obsd 473.1608.

Synthesis of 26. *Step 1:4-(3-Bromobenzyl)thiophene-2-carbaldehyde (**I-42**).* To a degassed solution of 2-formyl-4-thiopheneboronic acid (500 mg, 3.21 mmol), 3-bromobenzyl bromide (0.88 g, 3.53 mmol), and K_2CO_3(1.33 g, 9.6 mmol) in 1,4-dioxane (15 mL) was added $Pd(PPh_3)_4$ (0.185 g, 0.16 mmol). The reaction mixture was stirred at 80 °C for 1 d and then quenched with water and extracted with EtOAc. The combined organic layers were dried over Mg_2SO_4, filtered, and concentrated in vacuo. The crude material was purified on silica gel to provide **I-42** (631 mg, 70%). ^{1}H NMR ($CDCl_3$) δ 9.86 (d, 1H, J = 1.2 Hz), 7.55 (d, 1H, J = 1.2 Hz), 7.42−7.32 (m, 3H), 7.20 (t, 1H, J = 7.7 Hz), 7.13 (d, 1H, J = 7.7 Hz), 3.97 (s, 2H). LCMS (FA): m/z = 282.9 (M+H).

*Step 2: rac-[4-(3-Bromobenzyl)-2-thienyl](4-chloropyrimidin-5-yl)methanol (**I-43**).* A solution of 4-chloro-5-iodopyrimidine (216 mg, 0.90 mmol) in THF (5.0 mL) was cooled to −78 °C with dry ice bath. To the solution was added dropwise 2.50 M of *n*-BuLi in hexane (0.36 mL, 0.90 mmol) at −78 °C, and the mixture was stirred for 20 min. To the mixture was added a solution of 4-(3-bromobenzyl)-thiophene-2-carbaldehyde (210 mg, 0.75 mmol) in THF (2.0 mL) at −78 °C, and the resulting mixture was stirred for 30 min. The reaction was quenched by addition of saturated NH_4Cl (50 mL) and extracted with EtOAc (50 mL) three times. The combined organic layers were dried over Na_2SO_4, filtered, and concentrated in vacuo. The crude product was purified on silica gel to provide **I-43** as a colorless oil (260 mg, 86%). ^{1}H NMR ($CDCl_3$) δ 9.02 (s, 1H), 8.94 (s, 1H), 7.35 (d, 1H, J = 7.9 Hz), 7.32 (s, 1H), 7.17 (t, 1H, J = 7.7 Hz), 7.09 (d, 1H, J = 7.7 Hz), 6.91 (s, 1H), 6.82 (s, 1H), 6.27 (s, 1H), 3.86 (s, 2H), 2.86−2.60 (br s, 1H). LCMS (FA): m/z = 396.9 (M+H).

*Step 3: [4-(3-Bromobenzyl)-2-thienyl](4-chloropyrimidin-5-yl)-methanone (**I-44**).* To a solution of rac-[4-(3-bromobenzyl)-2-thienyl](4-chloropyrimidin-5-yl)methanol (255 mg, 0.64 mmol) in DCM (10.0 mL) was added Dess−Martin periodinane (410 mg, 0.97 mmol) at rt, and the mixture was stirred for 15 min. The reaction was quenched by addition of saturated $NaHCO_3$ (50 mL) and extracted with DCM (50 mL) three times. The combined organic layers were washed with brine, dried over Na_2SO_4, filtered, and concentrated in vacuo. The residue was purified on silica gel to afford **I-44** as a colorless oil (247 mg, 96%). ^{1}H NMR ($CDCl_3$) δ 9.12 (s, 1H), 8.75 (s, 1H), 7.49−7.45 (m, 1H), 7.38 (d, 1H, J = 8.0 Hz), 7.31 (s, 1H), 7.28 (d, 1H, J = 1.4 Hz), 7.18 (t, 1H, J = 7.8 Hz), 7.09 (d, 1H, J = 7.8 Hz), 3.94 (s, 2H). LCMS (FA): m/z = 394.9 (M+H).

*Step 4: [4-(3-Bromobenzyl)-2-thienyl][4-({(1R,3R,4S)-3-({[tert-butyl(dimethyl)silyl]oxy}methyl)-4-[(triisopropylsilyl)oxy]-cyclopentyl}amino)pyrimidin-5-yl]methanone (**I-45**).* To a solution of [4-(3-bromobenzyl)-2-thienyl](4-chloropyrimidin-5-yl)methanone (245 mg, 0.62 mmol) in DMF (10 mL) was added (1*R*,3*R*,4*S*)-3-({[*tert*-butyl(dimethyl)silyl]oxy}methyl)-4-[(triisopropylsilyl)oxy]-cyclopentanamine (**I-31**, 375 mg, 0.93 mmol) followed by K_2CO_3 (215 mg, 1.56 mmol), and the reaction was stirred for 13 h at rt. The reaction was concentrated in vacuo. To the residue was added water (50 mL) and the mixture was extracted with EtOAc (50 mL) three times. The combined organic layers were dried over Na_2SO_4, filtered, and concentrated in vacuo. The residue was purified on silica gel to give **I-45** as a light yellow oil (445 mg, 94%). ^{1}H NMR ($CDCl_3$) δ 8.78 (s, 1H), 8.69−8.56 (m, 2H), 7.42−7.30 (m, 4H), 7.18 (t, 1H, J = 7.7 Hz), 7.12 (d, 1H, J = 7.7 Hz), 4.86−4.72 (m, 1H), 4.33−4.25 (m, 1H), 3.96 (s, 2H), 3.61 (dd, 1H, J = 10.1, 5.4 Hz), 3.55 (dd, 1H, J = 10.1, 5.8 Hz), 2.49−2.36 (m, 1H), 2.24−2.08 (m, 2H), 1.77−1.66 (m, 1H), 1.34−1.17 (m, 1H), 1.06 (s, 21H), 0.88 (s, 9H), 0.03 (s, 6H).

*Step 5: [4-(3-Bromobenzyl)-2-thienyl][4-({(1R,3R,4S)-3-(hydroxymethyl)-4-[(triisopropylsilyl)oxy]cyclopentyl}amino)pyrimidin-5-yl]-methanone (**I-46**).* To a solution of [4-(3-bromobenzyl)-2-thienyl][4-({(1*R*,3*R*,4*S*)-3-({[*tert*-butyl(dimethyl)silyl]oxy}methyl)-4-[(triisopropylsilyl)oxy]cyclopentyl}amino)pyrimidin-5-yl]methanone (150 mg, 0.20 mmol) in EtOH (8.0 mL) was added 1% HCl in EtOH solution (2.0 mL, 0.24 mmol), and the mixture was stirred for 8 h at rt. The reaction was quenched by addition of saturated $NaHCO_3$ (50 mL) and extracted with EtOAc (60 mL) three times. The combined organic layers were washed with brine, dried over Na_2SO_4, filtered, and concentrated in vacuo. The residue was purified on silica gel to provide **I-46** as a light yellow oil (113 mg, 89%). ^{1}H NMR ($CDCl_3$) δ 8.79 (s, 1H), 8.71 (d, 1H, J = 7.3 Hz), 8.66 (s, 1H), 7.40−7.32 (m, 4H), 7.19 (dd, 1H, J = 7.8, 7.6 Hz), 7.15−7.11 (m, 1H), 4.86−4.76 (m, 1H), 4.35−4.30 (m, 1H), 3.97 (s, 2H), 3.74−3.66 (m, 2H), 2.54−2.45 (m, 1H), 2.24−2.15 (m, 2H), 1.89−1. 81 (m, 1H), 1.75 (t, 1H, J = 4.8 Hz), 1.32 (dt, 1H, J = 13.2, 7.8 Hz), 1.10−1.04 (m, 21H). LCMS (FA): m/z = 646.1 (M+H).

*Step 6: {(1R,2S,4R)-4-[(5-{[4-(3-Bromobenzyl)-2-thienyl]-carbonyl}pyrimidin-4-yl)amino]-2-[(triisopropylsilyl)oxy]-cyclopentyl}methyl sulfamate (**I-47**).* To a solution of [4-(3-bromobenzyl)-2-thienyl][4-({(1*R*,3*R*,4*S*)-3-(hydroxymethyl)-4-[(triisopropylsilyl)oxy]cyclopentyl}amino)pyrimidin-5-yl]methanone (110 mg, 0.17 mmol) in DMF (2.0 mL) was added chlorosulfonamide (39.4 mg, 0.34 mmol) at rt, and the mixture was stirred for 15 min. The reaction was cooled to 0 °C and quenched by addition of saturated $NaHCO_3$ (50 mL). The mixture was extracted with EtOAc (50 mL) three times. The combined organic layers were dried over Na_2SO_4, filtered, and concentrated in vacuo. The residue was purified on silica

https://dx.doi.org/10.1021/acs.jmedchem.0c01491
J. Med. Chem. 2021, 64, 2501−2520

gel to give **I-47** as a light yellow sticky oil (101 mg, 78%). ^{1}H NMR ($CDCl_3$) δ 8.79 (s, 1H), 8.72−8.59 (m, 2H), 7.45−7.30 (m, 4H), 7.19 (t, 1H, J = 7.7 Hz), 7.12 (d, 1H, J = 7.5 Hz), 5.15 (s, 2H), 4.88−4.75 (m, 1H), 4.34 (q, 1H, J = 5.2 Hz), 4.27 (d, 2H, J = 4.7 Hz), 3.96 (s, 2H), 2.67−2.53 (m, 1H), 2.43−2.30 (m, 1H), 2.22−2.11 (m, 1H), 1.90 (dt, 1H, J = 13.1, 6.4 Hz), 1.46 (dt, 1H, J = 13.2, 6.6 Hz), 1.05 (s, 21H). LCMS (FA): m/z = 725.1 (M+H).

*Step 7: {(1R,2S,4R)-4-[(5-{[4-(3-Bromobenzyl)-2-thienyl]carbonyl}pyrimidin-4-yl)amino]-2-hydroxycyclopentyl}methyl sulfamate (**26**).* To a solution of {(1*R*,2*S*,4*R*)-4-[(5-{[4-(3-bromobenzyl)-2-thienyl]carbonyl}pyrimidin-4-yl)amino]-2-[(triisopropylsilyl)oxy]cyclopentyl}methyl sulfamate (95.0 mg, 0.13 mmol) in THF (2.0 mL) was added 4.0 M of HCl (2.00 mL, 8.00 mmol) at rt, and the mixture was stirred for 4 h. The reaction was quenched by addition of saturated $NaHCO_3$ (60 mL) and extracted with EtOAc (60 mL) three times. The combined organic layers were washed with brine, dried over Na_2SO_4, filtered, and concentrated in vacuo. The residue was purified on silica gel to provide **26** as an off-white solid (66 mg, 87%). ^{1}H NMR (DMSO-d_6) δ 8.68 (s, 1H), 8.64 (s, 1H), 8.26 (d, 1H, J = 7.4 Hz), 7.82 (s, 1H), 7.70 (s, 1H), 7.51 (s, 1H), 7.48−7.35 (m, 3H), 7.35−7.20 (m, 2H), 4.88 (d, 1H, J = 4.5 Hz), 4.77−4.62 (m, 1H), 4.09 (dd, 1H, J = 9.6, 6.1 Hz), 4.04−3.87 (m, 4H), 2.31 (dt, 1H, J = 13.6, 7.5 Hz), 2.17−2.05 (m, 1H), 2.01−1.90 (m, 1H), 1.82−1.70 (m, 1H), 1.33−1.20 (m, 1H). LCMS (FA): m/z = 569.1 (M+H). HRMS m/z [M + H]$^+$ calcd for $C_{22}H_{24}BrN_4O_5S_2$ 567.0371, obsd 567.0370.

Synthesis of Intermediate I-107. *Step 1: [2-(2-{[tert-Butyl(dimethyl)silyl]oxy}ethyl)phenyl][5-(1,3-dioxolan-2-yl)- 2-methyl-3-thienyl]methanol (**I-106**).* A solution of 2-(4-bromo-5-methyl-2-thienyl)-1,3-dioxolane (1.70 g, 6.82 mmol) in THF (26.6 mL) was cooled to −78 °C, and then 2.50 M of *n*-BuLi in hexane (2.94 mL, 7.35 mmol) was added and the mixture was stirred for 10 min at −78 °C. A solution of 2-(2-{[*tert*-butyl(dimethyl)silyl]oxy}ethyl)benzaldehyde (**I-105**, 1.39 g, 5.25 mmol) in THF (13.3 mL) was then added, and the reaction was stirred for 10 min at −78 °C. The reaction was quenched by adding brine and then warmed to rt. The aqueous mixture was extracted with EtOAc twice. The combined organic solvents were washed with brine, dried, and concentrated in vacuo. The residue was purified on silica gel to provide **I-106** (1.96 g, 86%). ^{1}H NMR ($CDCl_3$) δ 7.30−7.26 (m, 2H), 7.26−7.21 (m, 2H), 7.07 (s, 1H), 6.09 (d, 1H, J = 2.7 Hz), 6.03 (s, 1H), 4.19−4.13 (m, 2H), 4.06−4.00 (m, 2H), 3.96−3.89 (m, 1H), 3.87−3.77 (m, 1H), 3.52 (d, 1H, J = 2.9 Hz), 3.06 (ddd, 1H, J = 14.3, 8.4, 6.2 Hz), 2.87 (dt, 1H, J = 13.9, 5.2 Hz), 2.37 (s, 3H), 0.86 (s, 9H), −0.00 (s, 3H), −0.01 (s, 3H).

*Step 2: 4-(3,4-Dihydro-1H-isochromen-1-yl)-5-methylthiophene-2-carbaldehyde (**I-107**).* A 100 mL round-bottom flask was charged with [2-(2-{[*tert*-butyl(dimethyl)silyl]oxy}ethyl)phenyl][5-(1,3-dioxolan-2-yl)-2-methyl-3-thienyl]methanol (1.96 g, 4.51 mmol) and TFA (6.60 mL, 85.7 mmol) at rt. The resulting purple solution was stirred at rt overnight. The reaction mixture was carefully poured into saturated aqueous $NaHCO_3$ (50 mL). The layers were separated, and the aqueous layer was extracted three times with EtOAc. The combined organic layers were washed with brine, then dried over sodium sulfate, filtered, and concentrated in vacuo. The residue was purified on silica gel to yield **I-107** (1.03 g, 89%). ^{1}H NMR ($CDCl_3$) δ 9.73 (s, 1H), 7.41 (s, 1H), 7.27−7.19 (m, 2H), 7.18−7.12 (m, 1H), 6.75 (d, 1H, J = 7.7 Hz), 5.86 (s, 1H), 4.21 (ddd, 1H, J = 11.3, 5.5, 3.7 Hz), 3.97 (ddd, 1H, J = 11.4, 9.7, 4.0 Hz), 3.16 (ddd, 1H, J = 15.9, 9.4, 5.4 Hz), 2.85 (dt, 1H, J = 16.6, 3.6 Hz), 2.59 (s, 3H).

Synthesis of Intermediate I-117. *Step 1: 1-[5-(1,3-Dioxolan-2-yl)-3-thienyl]-1,2,3,4-tetrahydroisoquinoline (**I-115**).* A solution of 3,4-dihydroisoquinoline (500 mg, 3.81 mmol) in THF (15.4 mL) was cooled at −30 °C. To this solution was added dropwise boron trifluoride etherate (0.53 mL, 4.19 mmol) at −30 °C, and the mixture was stirred for 20 min. Into a separate 50 mL 2-neck flask 2.50 M of *n*-BuLi in hexane (1.83 mL, 4.57 mmol) was added at −78 °C followed by a solution of 2-(4-bromo-2-thienyl)-1,3-dioxolane (1.08 g, 4.57 mmol) in THF (10 mL). After 5 min, lithiated thiophene suspension was added to the above solution of dihydroisoquinoline BF_3−OEt_2 complex at −78 °C. The reaction was stirred for 20 min at −78 °C and then quenched by addition of water. The layers were separated, and the aqueous layer was extracted with EtOAc. The combined organic layers were dried over Na_2SO_4, filtered, and concentrated in vacuo. The residue was purified on silica gel to provide **I-115** (513 mg) and some impurities as a red amorphous solid. This mixture was used for the next step without further purification.

*Step 2: tert-Butyl 1-[5-(1,3-Dioxolan-2-yl)-3-thienyl]-3,4-dihydroisoquinoline-2(1H)-carboxylate (**I-116**).* The crude mixture from step 1was dissolved in MeCN (6.97 mL), to which was added $(Boc)_2O$ (1.25 g, 5.72 mmol) and DMAP (2.33 mg, 19.1 μmol) at rt. After stirring for 2 h, the reaction was quenched by adding water. The layers were separated, and the aqueous layer was extracted with EtOAc twice. The combined organics were washed with brine, dried over Na_2SO_4, filtered, and concentrated in vacuo. The residue was purified on silica gel to provide **I-116** (393 mg, 27% for 2 steps). ^{1}H NMR ($CDCl_3$) δ 7.26−7.03 (m, 6H), 6.82 (s, 1H), 6.01 (s, 1H), 4.17−3.93 (m, 5H), 3.20−3.04 (m, 1H), 3.04−2.86 (m, 1H), 2.79−2.68 (m, 1H), 1.57−1.46 (m, 9H); LCMS (FA): m/z = 388.3 (M+H).

*Step 3: tert-Butyl 1-(5-Formyl-3-thienyl)-3,4-dihydroisoquinoline-2(1H)-carboxylate (**I-117**).* To a solution of *tert*-butyl 1-[5-(1,3-dioxolan-2-yl)-3-thienyl]-3,4-dihydroisoquinoline-2(1*H*)-carboxylate (393 mg, 1.01 mmol) in acetone (7.72 mL) was added 500 mg of Dowex 50WX-2-200 (H) (acid resin), and the mixture was shaken for 18 h at rt. The reaction was filtered through a glass frit funnel and the residual resin was rinsed with acetone several times. To the filtrate was added saturated aqueous $NaHCO_3$ (25 mL) and the mixture was concentrated to half volume in vacuo. The residue was diluted with EtOAc; the layers were separated, and the aqueous layer was extracted with EtOAc. The combined organic layers were dried over Na_2SO_4, filtered, and concentrated in vacuo. The residue was purified on silica gel to provide **I-117** as a colorless amorphous solid (319 mg, 91%). ^{1}H NMR ($CDCl_3$) δ 9.84 (s, 1H), 7.64 (s, 1H), 7.30−7.07 (m, 5H), 6.48−6.23 (br s, 1H), 4.09−3.88 (m, 1H), 3.22−3.06 (m, 1H), 3.05−2.89 (m, 1H), 2.81−2.69 (m, 1H), 1.52 (s, 9H).

■ ASSOCIATED CONTENT

Supporting Information

The Supporting Information is available free of charge at https://pubs.acs.org/doi/10.1021/acs.jmedchem.0c01491.

Molecular formula strings file and some data (CSV)

Protocols for the in vitro and cell assays and in vivo experiments, synthetic methods for the remaining examples, HPLC traces of final compound, protein synthesis and purification methodology, and X-ray crystallographic and microelectron diffraction protocols (PDF)

Accession Codes

PDB depositions are available for SAE SUMO adducts of compounds **2**, **46**, **49**, and TAK-981. The authors will release the atomic coordinates and experimental data upon article publication.

■ AUTHOR INFORMATION

Corresponding Authors

Steven P. Langston − *Millennium Pharmaceuticals, a wholly owned subsidiary of Takeda Pharmaceuticals Company Ltd., Cambridge, Massachusetts 02139, United States;* orcid.org/0000-0001-5840-0005; Email: steve.langston@takeda.com

Stephen Grossman − *Millennium Pharmaceuticals, a wholly owned subsidiary of Takeda Pharmaceuticals Company Ltd., Cambridge, Massachusetts 02139, United States;* Email: Stephen.Grossman@Takeda.com

https://dx.doi.org/10.1021/acs.jmedchem.0c01491
J. Med. Chem. 2021, 64, 2501−2520

Authors

Dylan England − *Millennium Pharmaceuticals, a wholly owned subsidiary of Takeda Pharmaceuticals Company Ltd., Cambridge, Massachusetts 02139, United States*

Roushan Afroze − *Millennium Pharmaceuticals, a wholly owned subsidiary of Takeda Pharmaceuticals Company Ltd., Cambridge, Massachusetts 02139, United States*

Neil Bence − *Millennium Pharmaceuticals, a wholly owned subsidiary of Takeda Pharmaceuticals Company Ltd., Cambridge, Massachusetts 02139, United States*

Douglas Bowman − *Millennium Pharmaceuticals, a wholly owned subsidiary of Takeda Pharmaceuticals Company Ltd., Cambridge, Massachusetts 02139, United States*

Nancy Bump − *Millennium Pharmaceuticals, a wholly owned subsidiary of Takeda Pharmaceuticals Company Ltd., Cambridge, Massachusetts 02139, United States*

Ryan Chau − *Millennium Pharmaceuticals, a wholly owned subsidiary of Takeda Pharmaceuticals Company Ltd., Cambridge, Massachusetts 02139, United States*

Bei-Ching Chuang − *Millennium Pharmaceuticals, a wholly owned subsidiary of Takeda Pharmaceuticals Company Ltd., Cambridge, Massachusetts 02139, United States*

Christopher Claiborne − *Millennium Pharmaceuticals, a wholly owned subsidiary of Takeda Pharmaceuticals Company Ltd., Cambridge, Massachusetts 02139, United States*

Larry Cohen − *Millennium Pharmaceuticals, a wholly owned subsidiary of Takeda Pharmaceuticals Company Ltd., Cambridge, Massachusetts 02139, United States; Takeda Pharmaceuticals, Fujisawa, Kanagawa 251-0012, Japan*

Kelly Connolly − *Millennium Pharmaceuticals, a wholly owned subsidiary of Takeda Pharmaceuticals Company Ltd., Cambridge, Massachusetts 02139, United States*

Matthew Duffey − *Millennium Pharmaceuticals, a wholly owned subsidiary of Takeda Pharmaceuticals Company Ltd., Cambridge, Massachusetts 02139, United States; Takeda Pharmaceuticals, Fujisawa, Kanagawa 251-0012, Japan*

Nitya Durvasula − *Millennium Pharmaceuticals, a wholly owned subsidiary of Takeda Pharmaceuticals Company Ltd., Cambridge, Massachusetts 02139, United States; Takeda Pharmaceuticals, Fujisawa, Kanagawa 251-0012, Japan*

Scott Freeze − *Millennium Pharmaceuticals, a wholly owned subsidiary of Takeda Pharmaceuticals Company Ltd., Cambridge, Massachusetts 02139, United States; Takeda Pharmaceuticals, Fujisawa, Kanagawa 251-0012, Japan*

Melissa Gallery − *Millennium Pharmaceuticals, a wholly owned subsidiary of Takeda Pharmaceuticals Company Ltd., Cambridge, Massachusetts 02139, United States; Takeda Pharmaceuticals, Fujisawa, Kanagawa 251-0012, Japan*

Katherine Galvin − *Millennium Pharmaceuticals, a wholly owned subsidiary of Takeda Pharmaceuticals Company Ltd., Cambridge, Massachusetts 02139, United States*

Jeffrey Gaulin − *Millennium Pharmaceuticals, a wholly owned subsidiary of Takeda Pharmaceuticals Company Ltd., Cambridge, Massachusetts 02139, United States*

Rachel Gershman − *Millennium Pharmaceuticals, a wholly owned subsidiary of Takeda Pharmaceuticals Company Ltd., Cambridge, Massachusetts 02139, United States*

Paul Greenspan − *Millennium Pharmaceuticals, a wholly owned subsidiary of Takeda Pharmaceuticals Company Ltd., Cambridge, Massachusetts 02139, United States*

Jessica Grieves − *Millennium Pharmaceuticals, a wholly owned subsidiary of Takeda Pharmaceuticals Company Ltd., Cambridge, Massachusetts 02139, United States*

Jianping Guo − *Millennium Pharmaceuticals, a wholly owned subsidiary of Takeda Pharmaceuticals Company Ltd., Cambridge, Massachusetts 02139, United States*

Nanda Gulavita − *Millennium Pharmaceuticals, a wholly owned subsidiary of Takeda Pharmaceuticals Company Ltd., Cambridge, Massachusetts 02139, United States*

Shumet Hailu − *Millennium Pharmaceuticals, a wholly owned subsidiary of Takeda Pharmaceuticals Company Ltd., Cambridge, Massachusetts 02139, United States*

Xingyue He − *Millennium Pharmaceuticals, a wholly owned subsidiary of Takeda Pharmaceuticals Company Ltd., Cambridge, Massachusetts 02139, United States*

Kara Hoar − *Millennium Pharmaceuticals, a wholly owned subsidiary of Takeda Pharmaceuticals Company Ltd., Cambridge, Massachusetts 02139, United States*

Yongbo Hu − *Millennium Pharmaceuticals, a wholly owned subsidiary of Takeda Pharmaceuticals Company Ltd., Cambridge, Massachusetts 02139, United States*

Zhigen Hu − *Millennium Pharmaceuticals, a wholly owned subsidiary of Takeda Pharmaceuticals Company Ltd., Cambridge, Massachusetts 02139, United States*

Mitsuhiro Ito − *Takeda Pharmaceuticals, Fujisawa, Kanagawa 251-0012, Japan*

Mi-Sook Kim − *Millennium Pharmaceuticals, a wholly owned subsidiary of Takeda Pharmaceuticals Company Ltd., Cambridge, Massachusetts 02139, United States*

Scott Weston Lane − *Millennium Pharmaceuticals, a wholly owned subsidiary of Takeda Pharmaceuticals Company Ltd., Cambridge, Massachusetts 02139, United States*

David Lok − *Millennium Pharmaceuticals, a wholly owned subsidiary of Takeda Pharmaceuticals Company Ltd., Cambridge, Massachusetts 02139, United States*

Anya Lublinsky − *Millennium Pharmaceuticals, a wholly owned subsidiary of Takeda Pharmaceuticals Company Ltd., Cambridge, Massachusetts 02139, United States*

William Mallender − *Millennium Pharmaceuticals, a wholly owned subsidiary of Takeda Pharmaceuticals Company Ltd., Cambridge, Massachusetts 02139, United States*

Charles McIntyre − *Millennium Pharmaceuticals, a wholly owned subsidiary of Takeda Pharmaceuticals Company Ltd., Cambridge, Massachusetts 02139, United States*

James Minissale − *Millennium Pharmaceuticals, a wholly owned subsidiary of Takeda Pharmaceuticals Company Ltd., Cambridge, Massachusetts 02139, United States*

Hirotake Mizutani − *Millennium Pharmaceuticals, a wholly owned subsidiary of Takeda Pharmaceuticals Company Ltd., Cambridge, Massachusetts 02139, United States*

Miho Mizutani − *Millennium Pharmaceuticals, a wholly owned subsidiary of Takeda Pharmaceuticals Company Ltd., Cambridge, Massachusetts 02139, United States*

Nina Molchinova − *Millennium Pharmaceuticals, a wholly owned subsidiary of Takeda Pharmaceuticals Company Ltd., Cambridge, Massachusetts 02139, United States*

Koji Ono − *Takeda Pharmaceuticals, Fujisawa, Kanagawa 251-0012, Japan*

Ashok Patil − *Millennium Pharmaceuticals, a wholly owned subsidiary of Takeda Pharmaceuticals Company Ltd., Cambridge, Massachusetts 02139, United States*

Mark Qian − *Millennium Pharmaceuticals, a wholly owned subsidiary of Takeda Pharmaceuticals Company Ltd., Cambridge, Massachusetts 02139, United States*

https://dx.doi.org/10.1021/acs.jmedchem.0c01491
J. Med. Chem. 2021, 64, 2501−2520

Jessica Riceberg − *Millennium Pharmaceuticals, a wholly owned subsidiary of Takeda Pharmaceuticals Company Ltd., Cambridge, Massachusetts 02139, United States*
Vaishali Shindi − *Millennium Pharmaceuticals, a wholly owned subsidiary of Takeda Pharmaceuticals Company Ltd., Cambridge, Massachusetts 02139, United States*
Michael D. Sintchak − *Millennium Pharmaceuticals, a wholly owned subsidiary of Takeda Pharmaceuticals Company Ltd., Cambridge, Massachusetts 02139, United States*
Keli Song − *Millennium Pharmaceuticals, a wholly owned subsidiary of Takeda Pharmaceuticals Company Ltd., Cambridge, Massachusetts 02139, United States*
Teresa Soucy − *Millennium Pharmaceuticals, a wholly owned subsidiary of Takeda Pharmaceuticals Company Ltd., Cambridge, Massachusetts 02139, United States*
Yana Wang − *Millennium Pharmaceuticals, a wholly owned subsidiary of Takeda Pharmaceuticals Company Ltd., Cambridge, Massachusetts 02139, United States*
He Xu − *Millennium Pharmaceuticals, a wholly owned subsidiary of Takeda Pharmaceuticals Company Ltd., Cambridge, Massachusetts 02139, United States*
Xiaofeng Yang − *Millennium Pharmaceuticals, a wholly owned subsidiary of Takeda Pharmaceuticals Company Ltd., Cambridge, Massachusetts 02139, United States*
Agatha Zawadzka − *Millennium Pharmaceuticals, a wholly owned subsidiary of Takeda Pharmaceuticals Company Ltd., Cambridge, Massachusetts 02139, United States*
Ji Zhang − *Millennium Pharmaceuticals, a wholly owned subsidiary of Takeda Pharmaceuticals Company Ltd., Cambridge, Massachusetts 02139, United States*
Sai M. Pulukuri − *Millennium Pharmaceuticals, a wholly owned subsidiary of Takeda Pharmaceuticals Company Ltd., Cambridge, Massachusetts 02139, United States*

Complete contact information is available at: https://pubs.acs.org/10.1021/acs.jmedchem.0c01491

Notes

The authors declare no competing financial interest.

■ ACKNOWLEDGMENTS

We would like to thank Dr. Dennis Huszar for reading the manuscript. We would like to thank Drs. John Ringeling, John Donovan, and Saurabh Menon for advice on assay development. We would also like to thank NanoImaging Inc. for performing the microED data collection.

■ ABBREVIATIONS USED

BID x21, twice per day for 21 days; BID BIW, twice per day/twice per week; BID 2on-5off, twice per day on 2 consecutive days, followed by 5 nondosing days; CA, carbonic anhydrase; QD x21, once per day for 21 consecutive days; QD x3/week, Three consecutive dosing days followed by 4 nondosing days; SC, subcutaneously; DLBCL, diffuse large B-cell lymphoma; IHC, immunohistochemistry; IF, immunofluorescence; IFN, type 1 interferon; IV, intravenously; PD, pharmacodynamic; SCID, severe combined immune deficiency; SEM, standard error of the mean

■ REFERENCES

(1) Geiss-Friedlander, R. Concepts in sumoylation: a decade on. *Nat. Rev. Mol. Cell Biol.* **2007**, *8* (12), 947−956.
(2) Schulman, B. A.; Harper, J. W. Ubiquitin-like protein activation by E1 enzymes: the apex for downstream signalling pathways. *Nat. Rev. Mol. Cell Biol.* **2009**, *10* (5), 319−331.
(3) Gareau, J. R.; Lima, C. D. The SUMO pathway: emerging mechanisms that shape specificity, conjugation and recognition. *Nat. Rev. Mol. Cell Biol.* **2010**, *11*, 861−871.
(4) Bernier-Villamor, V.; Sampson, D. A.; Matunis, M. J.; Lima, C. D. Structural basis for E2-mediated SUMO conjugation revealed by a complex between ubiquitin-conjugating enzyme Ubc9 and RanGAP1. *Cell* **2002**, *108* (3), 345−356.
(5) Johnson, E. S. Protein modification by SUMO. *Annu. Rev. Biochem.* **2004**, *73*, 355−382.
(6) Hershko, A.; Ciechanover, A. The ubiquitin system. *Annu. Rev. Biochem.* **1998**, *67*, 425−479.
(7) Gong, L.; Yeh, E. T. Identification of the activating and conjugating enzymes of the NEDD8 conjugation pathway. *J. Biol. Chem.* **1999**, *274* (17), 12036−12042.
(8) Bergink, S.; Jentsch, S. Principles of ubiquitin and SUMO modifications in DNA repair. *Nature* **2009**, *458* (7237), 461−467.
(9) Chen, S. F.; Gong, C.; Luo, M.; Yao, H. R.; Zeng, Y. J.; Su, F. X. Ubc9 expression predicts chemoresistance in breast cancer. *Aizheng* **2011**, *30* (9), 638−644.
(10) Seeler, J. S.; Dejean, A. SUMO and the robustness of cancer. *Nat. Rev. Cancer* **2017**, *17* (3), 184−197.
(11) Kessler, J. D.; Kahle, K. T.; Sun, T.; Meerbrey, K. L.; Schlabach, M. R.; Schmitt, E. M.; Skinner, S. O.; Xu, Q.; Li, M. Z.; Hartman, Z. C.; Rao, M.; Yu, P.; Dominguez-Vidana, R.; Liang, A. C.; Solimini, N. L.; Bernardi, R. J.; Yu, B.; Hsu, T.; Golding, I.; Luo, J.; Osborne, C. K.; Creighton, C. J.; Hilsenbeck, S. G.; Schiff, R.; Shaw, C. A.; Elledge, S. J.; Westbrook, T. F. A SUMOylation-dependent transcriptional subprogram is required for Myc-driven tumorigenesis. *Science* **2012**, *335*, 348−353.
(12) He, X.; Riceberg, J.; Pulukuri, S. M.; Grossman, S.; Shinde, V.; Shah, P.; Brownell, J. E.; Dick, L.; Newcomb, J.; Bence, N. Characterization of the loss of SUMO pathway function on cancer cells and tumor proliferation. *PLoS One* **2015**, *10* (4), No. e0123882.
(13) Liu, X.; Xu, Y.; Pang, Z.; Guo, F.; Qin, Q.; Yin, T.; Sang, Y.; Feng, C.; Li, X.; Jiang, L.; Shu, P.; Wang, Y. Knockdown of SUMO-activating enzyme subunit 2 (SAE2) suppresses cancer malignancy and enhances chemotherapy sensitivity in small cell lung cancer. *J. Hematol. Oncol.* **2015**, *8*, 1−10.
(14) Biederstadt, A.; Hassan, Z.; Schneeweis, C.; Schick, M.; Schneider, L.; Muckenhuber, A.; Hong, Y.; Siegers, G.; Nilsson, L.; Wirth, M.; Dantes, Z.; Steiger, K.; Schunck, K.; Langston, S.; Lenhof, H. P.; Coluccio, A.; Orben, F.; Slawska, J.; Scherger, A.; Saur, D.; Muller, S.; Rad, R.; Weichert, W.; Nilsson, J.; Reichert, M.; Schneider, G.; Keller, U. SUMO pathway inhibition targets an aggressive pancreatic cancer subtype. *Gut* **2020**, *8*, 1472−1482.
(15) Adorisio, S.; Fierabracci, A.; Muscari, I.; Liberati, A. M.; Ayroldi, E.; Migliorati, G.; Thuy, T. T.; Riccardi, C.; Delfino, D. V. SUMO proteins: Guardians of immune system. *J. Autoimmun.* **2017**, *84*, 21−28.
(16) Decque, A.; Joffre, O.; Magalhaes, J. G.; Cossec, J. C.; Blecher-Gonen, R.; Lapaquette, P.; Silvin, A.; Manel, N.; Joubert, P. E.; Seeler, J. S.; Albert, M. L.; Amit, I.; Amigorena, S.; Dejean, A. Sumoylation coordinates the repression of inflammatory and anti-viral gene-expression programs during innate sensing. *Nat. Immunol.* **2016**, *17* (2), 140−149.
(17) Crowl, J. T.; Stetson, D. B. SUMO2 and SUMO3 redundantly prevent a noncanonical type I interferon response. *Proc. Natl. Acad. Sci. U. S. A.* **2018**, *115* (26), 6798−6803.
(18) Brownell, J. E.; Sintchak, M. D.; Gavin, J. M.; Liao, H.; Bruzzese, F. J.; Bump, N. J.; Soucy, T. A.; Milhollen, M. A.; Yang, X.; Burkhardt, A. L.; Ma, J.; Loke, H. K.; Lingaraj, T.; Wu, D.; Hamman, K. B.; Spelman, J. J.; Cullis, C. A.; Langston, S. P.; Vyskocil, S.; Sells, T. B.; Mallender, W. D.; Visiers, I.; Li, P.; Claiborne, C. F.; Rolfe, M.; Bolen, J. B.; Dick, L. R. Substrate-assisted inhibition of ubiquitin-like protein-activating enzymes: the NEDD8 E1 inhibitor MLN4924 forms a NEDD8-AMP mimetic in situ. *Mol. Cell* **2010**, *37* (1), 102−111.

(19) Chen, J. J.; Tsu, C. A.; Gavin, J. M.; Milhollen, M. A.; Bruzzese, F. J.; Mallender, W. D.; Sintchak, M. D.; Bump, N. J.; Yang, X.; Ma, J.; Loke, H. K.; Xu, Q.; Li, P.; Bence, N. F.; Brownell, J. E.; Dick, L. R. Mechanistic studies of substrate-assisted inhibition of ubiquitin-activating enzyme by adenosine sulfamate analogues. *J. Biol. Chem.* **2011**, *286* (47), 40867−40877.
(20) Lu, X.; Olsen, S. K.; Capili, A. D.; Cisar, J. S.; Lima, C. D.; Tan, D. S. Designed semisynthetic protein inhibitors of Ub/Ubl E1 activating enzymes. *J. Am. Chem. Soc.* **2010**, *132* (6), 1748−1749.
(21) Olsen, S. K.; Capili, A. D.; Lu, X.; Tan, D. S.; Lima, C. D. Active site remodelling accompanies thioester bond formation in the SUMO E1. *Nature* **2010**, *463* (7283), 906−912.
(22) Swords, R. T.; Erba, H. P.; DeAngelo, D. J.; Bixby, D. L.; Altman, J. K.; Maris, M.; Hua, Z.; Blakemore, S. J.; Faessel, H.; Sedarati, F.; Dezube, B. J.; Giles, F. J.; Medeiros, B. C. Pevonedistat (MLN4924), a First-in-Class NEDD8-activating enzyme inhibitor, in patients with acute myeloid leukaemia and myelodysplastic syndromes: a phase 1 study. *Br. J. Haematol.* **2015**, *169* (4), 534−543.
(23) Mizutani, H.; Langston, S. P.; Vyskocil, S. Synthesis of a Potent NAE Inhibitor: Pevonedistat. In *Comprehensive Accounts of Pharmaceutical Research and Development: From Discovery to Late-Stage Process Development Vol. 2*; Ahmed, F. A.-M., Pesti, J. A.., Vaidyanathan, R., Eds.; ACS Symposium Series: 2016; Vol. *1240*, pp 1−11.
(24) Milhollen, M. A.; Traore, T.; Adams-Duffy, J.; Thomas, M. P.; Berger, A. J.; Dang, L.; Dick, L. R.; Garnsey, J. J.; Koenig, E.; Langston, S. P.; Manfredi, M.; Narayanan, U.; Rolfe, M.; Staudt, L. M.; Soucy, T. A.; Yu, J.; Zhang, J.; Bolen, J. B.; Smith, P. G. MLN4924, a NEDD8-activating enzyme inhibitor, is active in diffuse large B-cell lymphoma models: rationale for treatment of NF-{kappa}B-dependent lymphoma. *Blood* **2010**, *116* (9), 1515−1523.
(25) Soucy, T. A.; Smith, P. G.; Milhollen, M. A.; Berger, A. J.; Gavin, J. M.; Adhikari, S.; Brownell, J. E.; Burke, K. E.; Cardin, D. P.; Critchley, S.; Cullis, C. A.; Doucette, A.; Garnsey, J. J.; Gaulin, J. L.; Gershman, R. E.; Lublinsky, A. R.; McDonald, A.; Mizutani, H.; Narayanan, U.; Olhava, E. J.; Peluso, S.; Rezaei, M.; Sintchak, M. D.; Talreja, T.; Thomas, M. P.; Traore, T.; Vyskocil, S.; Weatherhead, G. S.; Yu, J.; Zhang, J.; Dick, L. R.; Claiborne, C. F.; Rolfe, M.; Bolen, J. B.; Langston, S. P. An inhibitor of NEDD8-activating enzyme as a new approach to treat cancer. *Nature* **2009**, *458* (7239), 732−736.
(26) Hyer, M. L.; Milhollen, M. A.; Ciavarri, J.; Fleming, P.; Traore, T.; Sappal, D.; Huck, J.; Shi, J.; Gavin, J.; Brownell, J.; Yang, Y.; Stringer, B.; Griffin, R.; Bruzzese, F.; Soucy, T.; Duffy, J.; Rabino, C.; Riceberg, J.; Hoar, K.; Lublinsky, A.; Menon, S.; Sintchak, M.; Bump, N.; Pulukuri, S. M.; Langston, S.; Tirrell, S.; Kuranda, M.; Veiby, P.; Newcomb, J.; Li, P.; Wu, J. T.; Powe, J.; Dick, L. R.; Greenspan, P.; Galvin, K.; Manfredi, M.; Claiborne, C.; Amidon, B. S.; Bence, N. F. A small-molecule inhibitor of the ubiquitin activating enzyme for cancer treatment. *Nat. Med.* **2018**, *24* (2), 186−193.
(27) Ciavarri, J.; Langston, S., The Discovery of First-in-Class Inhibitors of the Nedd8-Activating Enzyme (NAE) and the Ubiquitin-Activating Enzyme (UAE). In *Comprehensive Medicinal Chemistry III*, Chackalamannil, S., Rotella, D., Ward, S., Eds.; Elsevier: Oxford, 2017; Vol. *8*, pp 95−112.
(28) An, H.; Statsyuk, A. V. Development of activity-based probes for ubiquitin and ubiquitin-like protein signaling pathways. *J. Am. Chem. Soc.* **2013**, *135* (45), 16948−16962.
(29) Misra, M.; Kuhn, M.; Lobel, M.; An, H.; Statsyuk, A. V.; Sotriffer, C.; Schindelin, H. Dissecting the Specificity of Adenosyl Sulfamate Inhibitors Targeting the Ubiquitin-Activating Enzyme. *Structure* **2017**, *25* (7), 1120−1129.
(30) Fukuda, I.; Ito, A.; Hirai, G.; Nishimura, S.; Kawasaki, H.; Saitoh, H.; Kimura, K.; Sodeoka, M.; Yoshida, M. Ginkgolic acid inhibits protein SUMOylation by blocking formation of the E1-SUMO intermediate. *Chem. Biol.* **2009**, *16* (2), 133−140.
(31) Takemoto, M.; Kawamura, Y.; Hirohama, M.; Yamaguchi, Y.; Handa, H.; Saitoh, H.; Nakao, Y.; Kawada, M.; Khalid, K.; Koshino, H.; Kimura, K.; Ito, A.; Yoshida, M. Inhibition of protein SUMOylation by davidiin, an ellagitannin from Davidia involucrata. *J. Antibiot.* **2014**, *67* (4), 335−338.
(32) Fukuda, I.; Ito, A.; Uramoto, M.; Saitoh, H.; Kawasaki, H.; Osada, H.; Yoshida, M. Kerriamycin B inhibits protein SUMOylation. *J. Antibiot.* **2009**, *62* (4), 221−224.
(33) He, X.; Riceberg, J.; Soucy, T.; Koenig, E.; Minissale, J.; Gallery, M.; Bernard, H.; Yang, X.; Liao, H.; Rabino, C.; Shah, P.; Xega, K.; Yan, Z. H.; Sintchak, M.; Bradley, J.; Xu, H.; Duffey, M.; England, D.; Mizutani, H.; Hu, Z.; Guo, J.; Chau, R.; Dick, L. R.; Brownell, J. E.; Newcomb, J.; Langston, S.; Lightcap, E. S.; Bence, N.; Pulukuri, S. M. Probing the roles of SUMOylation in cancer cell biology by using a selective SAE inhibitor. *Nat. Chem. Biol.* **2017**, *13* (11), 1164−1171.
(34) Lv, Z.; Williams, K. M.; Yuan, L.; Atkison, J. H.; Olsen, S. K. Crystal structure of a human ubiquitin E1-ubiquitin complex reveals conserved functional elements essential for activity. *J. Biol. Chem.* **2018**, *293* (47), 18337−18352.
(35) Minissale, J.; Burkhardt, A. Unpublished results.
(36) Shank, R. P.; Doose, D. R.; Streeter, A. J.; Bialer, M. Plasma and whole blood pharmacokinetics of topiramate: the role of carbonic anhydrase. *Epilepsy Res.* **2005**, *63* (2−3), 103−112.
(37) Winum, J. Y.; Scozzafava, A.; Montero, J. L.; Supuran, C. T. Sulfamates and their therapeutic potential. *Med. Res. Rev.* **2005**, *25* (2), 186−228.
(38) Lightcap, Y. P.; Grossman, S.; Song, K.; Khattar, M.; Xega, K.; He, X.; Gavin, J. G.; Imaichi, H.; Garnsey, J. J.; Koenig, E.; Zhang, H.; Lu, Z.; Shah, P.; Hatton, B. A.; Riceberg, J.; Shinde, V.; Li, C.; Minissale, J.; Yang, X.; England, D.; Klinghoffer, R. A.; Langston, S.; Galvin, K.; Shapiro, G.; Pulukuri, S. M.; Fuchs, S. Y.; Huszar, D. Unpublished results.
(39) Huszar, D. *TAK-981: A first-in-class SUMOylation inhibitor in phase 1 clinical trials promotes a Type I interferon response and antitumor immunity in preclinical models*, Session DDT01; American Association for Cancer Research: Atlanta, GA, Mar 29−Apr 03, 2019.
(40) Li, Y. J.; Du, L.; Wang, J.; Vega, R.; Lee, T. D.; Miao, Y.; Aldana-Masangkay, G.; Samuels, E. R.; Li, B.; Ouyang, S. X.; Colayco, S. A.; Bobkova, E. V.; Divlianska, D. B.; Sergienko, E.; Chung, T. D. Y.; Fakih, M.; Chen, Y. Allosteric Inhibition of Ubiquitin-like Modifications by a Class of Inhibitor of SUMO-Activating Enzyme. *Cell Chem. Biol.* **2019**, *26* (2), 278−288.
(41) Lv, Z.; Yuan, L.; Atkison, J. H.; Williams, K. M.; Vega, R.; Sessions, E. H.; Divlianska, D. B.; Davies, C.; Chen, Y.; Olsen, S. K. Molecular mechanism of a covalent allosteric inhibitor of SUMO E1 activating enzyme. *Nat. Commun.* **2018**, *9*, 1−12.

https://dx.doi.org/10.1021/acs.jmedchem.0c01491
J. Med. Chem. 2021, 64, 2501−2520